

# Less is More: Token-Efficient Video-QA via Adaptive Frame-Pruning and Semantic Graph Integration

Shaoguang Wang<sup>1</sup> Weiyu Guo<sup>1</sup> Ziyang Chen<sup>1</sup> Yijie Xu<sup>1</sup> Xuming Hu<sup>1,\*</sup> Hui Xiong<sup>1,2,\*</sup>

<sup>1</sup>Thrust of Artificial Intelligence, HKUST (Guangzhou), China

<sup>2</sup>Department of Computer Science and Engineering, HKUST, Hong Kong SAR, China

swang440@connect.hkust-gz.edu.cn, xuminghu@hkust-gz.edu.cn, xionghui@ust.hk

## Abstract

The practical application of Multimodal Large Language Models (MLLMs) to Video Question Answering (Video-QA) is severely hindered by the high token cost of processing numerous video frames. While keyframe selection is the dominant strategy for mitigating this, we identify that even state-of-the-art selectors produce prompts laden with significant temporal redundancy, a challenge unique to video that we term ‘visual echoes’. This issue leads to context dilution and can paradoxically degrade performance. To address this dual challenge, we propose a novel refinement framework that synergistically combines **Adaptive Frame-Pruning (AFP)** with a lightweight text-based semantic graph. **AFP** intelligently prunes ‘visual echoes’ by adaptively clustering frames, while the semantic graph provides crucial, low-cost semantic compensation. Conducting extensive experiments on the LONGVIDEOBENCH and VIDEOMME benchmarks against multiple state-of-the-art selectors, our approach demonstrates a drastic reduction in total input tokens by up to 80%. Crucially, by creating a concise, high-quality prompt, our framework not only enhances efficiency but also demonstrates a remarkable ability to robustify and improve the accuracy of upstream selectors, achieving results that are highly competitive with, and often superior to, baselines that use vastly more frames. Code will be made publicly available.

## 1. Introduction

The advent of Multimodal Large Language Models (MLLMs), such as GPT-4o, Gemini, Video-ChatGPT, MovieChat, and Video-LLaVA [10, 16, 19, 29, 32], has led to a clear change in vision–language understanding. These models show strong ability in handling complex reasoning over visual and textual inputs, with Video Question Answer-

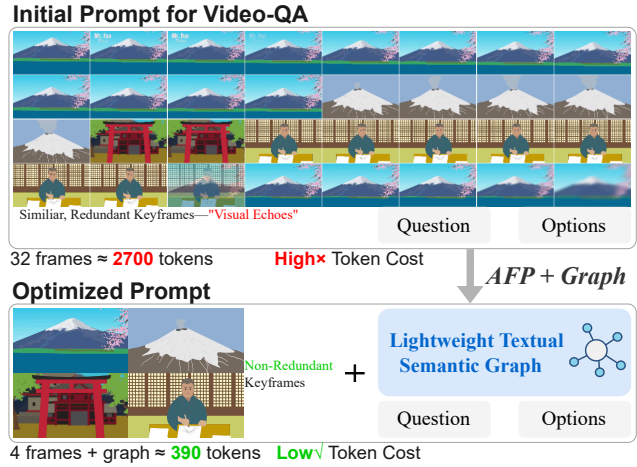


Figure 1. **Conceptual Overview of our Refinement Framework.** (a) An initial prompt from an upstream selector contains numerous ‘visual echoes’ and has a high token cost. (b) Our framework refines this by pruning redundant frames with **AFP** and compensating with a semantic graph, resulting in an optimized, low-cost prompt that leads to the correct answer. *Token counts are illustrative estimates based on OpenAI’s guidelines (see Section 4.1).*

ing (Video-QA) becoming an important application. However, their use in the video domain is limited by the very high token cost. This issue is critical for long videos; for example, sampling a one-hour video at 1 fps produces 3,600 frames, resulting in a token count that far exceeds the context window of current MLLMs. This makes naive frame sampling ineffective and highlights the need for more selective frame sampling strategies.

This computational barrier forces a departure from naive sampling strategies. While dense uniform sampling is infeasible, simply resorting to a sparse, fixed sampling (e.g., 32 frames for a long video) is equally problematic. Such a *query-agnostic* approach is fundamentally unreliable, as it runs a high risk of missing the brief but decisive moments essential for answering the specific question posed.

Consequently, *query-aware* keyframe selection has

\*Corresponding authors.

Arxiv Preprint.



Figure 2. “Visual Echoes” are a Prevalent Issue Across Mainstream Keyframe Selectors. We visualize 32 keyframes selected by three SOTA methods for a video QA task involving narrative understanding. All selectors exhibit severe redundancy, producing multiple near-identical frames for iconic subjects. We use colored bounding boxes to highlight these clusters of “visual echoes,” such as the Fuji mountain view, the seated man, and the red Torii gate.

emerged as a dominant and essential preprocessing paradigm. Yet, this approach introduces a critical trade-off. To ensure no relevant information is missed (i.e., to maximize recall), state-of-the-art selectors are designed to be comprehensive, often returning a generous and often redundant set of candidate frames for downstream analysis.

This inherent design choice leads to two significant, often-overlooked challenges. First, due to the temporal coherency of video, the selected keyframes inevitably contain significant redundancy, which we term ‘**visual echoes**’: temporally proximate frames with high visual similarity (illustrated conceptually in Figure 1). For additional examples demonstrating this issue across diverse video types, including scientific animations and real-world footage, please see Appendix C. This tendency is not an isolated flaw of a particular method, but a widespread issue across the current paradigm, as we demonstrate in Figure 2 where multiple leading selectors exhibit this behavior. Second, the overabundance of visual information, even if relevant, leads to ‘**context dilution**’, which can introduce noise and overwhelm the MLLM’s reasoning capacity. These twin challenges hinder the potential for a “less is more” paradigm, often leading to a counter-intuitive outcome where more frames do not necessarily yield better results, as noted in recent literature [18].

These observations lead us to a more refined research question: *How can we refine a redundant and noisy set of initial keyframes into an optimal, token-efficient prompt that is both visually concise and semantically complete?*

To answer this question, we propose a novel, two-pronged framework that synergistically combines **Adaptive Frame-Pruning (AFP)** and a **text-based semantic graph**. As illustrated in our conceptual overview (Figure 1), our framework operates as a universal refinement layer. The **AFP** module directly tackles the ‘visual echoes’ problem by employing an adaptive clustering algorithm to merge redundant frames into a concise visual foundation. Concurrently, the lightweight semantic graph compensates for potential information loss that occurs during pruning. It provides a structured, low-cost summary of key entities and their relationships, ensuring that essential semantic context is preserved and highlighted for the MLLM. Together, they transform a high-cost, cluttered prompt into a highly efficient and effective one. To summarize, the main contributions of our work are threefold:

- We formally define and demonstrate the prevalence of ‘**visual echoes**’ in video, and attribute the ‘less is more’ paradox observed in Video-QA to this issue and the challenge of ‘**context dilution**’.
- We propose a novel, two-pronged framework that combines **AFP** with a lightweight, text-based semantic graph to act as a universal refinement module for any SOTA keyframe selector.
- We conduct extensive experiments on the LONG VIDEOBENCH and VIDEOMME benchmarks across different baselines and models, demonstrating that our dual-strategy approach not only drastically reduces token costs but also frequently improves accuracy, thereby robustifying upstream selectors.

## 2. Related Work

**MLLMs for Video Understanding.** The application of MLLMs to video understanding has seen rapid evolution through diverse paradigms. Early approaches utilized LLMs as high-level planners to generate executable code for video analysis [30, 37]. A dominant paradigm then emerged, focusing on direct visual-language alignment by connecting video encoders to LLMs via projection layers, enabling conversational abilities [4, 16, 19, 45, 48]. To handle long-form videos, methods like MovieChat introduced memory mechanisms [29, 36], while others combined visual features with textual signals like ASR/OCR for dense spatiotemporal tasks [17, 40]. More specialized adaptations have appeared, such as transforming LLMs into planners that iteratively call visual tools [33], regression models for timestamp prediction [9, 26], or efficient pipelines that leverage video analyzers to generate rich text descriptions for frozen LLMs [47].

**Keyframe Selection for Video Understanding.** A common thread uniting the aforementioned methods when applied to long videos is the prohibitive token cost. Consequently, keyframe selection has emerged as a crucial and dominant preprocessing paradigm [1, 10, 32]. Approaches to query-aware keyframe selection have diversified into several dis-

tinct families. One major family relies on *clustering* frames based on visual or semantic similarity to find representative moments, with methods like VideoTree being a prominent example [11, 22, 27, 34, 44]. Another popular paradigm frames the task as an *agent-based* search, where the LLM iteratively interacts with the video to locate relevant information [5, 14, 33, 38, 43]. A third, more recent school of thought focuses on direct *temporal* search and optimization, developing sophisticated, often training-free, scoring mechanisms to pinpoint keyframes directly. State-of-the-art selectors like  $T^*$  [42], VSLS [7], and AKS [31] exemplify this approach [15]. Existing keyframe selectors, in their pursuit of high recall, suffer from two pitfalls: 1) generating redundant ‘visual echoes’ that dilute context, and 2) the risk of losing semantic information during pruning. Our framework is designed to resolve both, using adaptive pruning to tackle redundancy and a semantic graph for compensation.

**Addressing Redundancy and Semantic Gaps.** Approaches to address temporal redundancy in video operate at various levels. While methods like TRIM [28] perform patch-level token reduction within frames, our work is positioned at the frame level, consolidating entire redundant frames (“visual echoes”). To compensate for the potential semantic gap left by such pruning, a prominent paradigm is the use of structured semantic representations. A foundational approach in this area is the scene graph [12], which provides a rich, structured vocabulary of objects and their inter-relationships. However, reasoning over these detailed graphs often necessitates complex Graph Neural Network (GNN) architectures [39]. More recent frameworks, such as CROSS [46], have explored modeling dynamic Temporal Text-attributed Graphs (TTAGs), demonstrating a trend towards integrating semantic and structural information over time. In contrast to these methods, our work introduces a lightweight text-attributed semantic graph specifically designed for minimal overhead. By injecting structured context directly into the MLLM’s prompt, it serves as a highly compatible compensation mechanism without requiring specialized GNNs, aligning with maximum token efficiency.

### 3. Methodology

Our approach enhances Video Understanding efficiency via a two-pronged strategy of **Pruning and Compensation**. We first prune the visual stream to a concise, non-redundant keyframe set, then compensate for information loss by injecting an efficient, abstract semantic layer. The two main stages, illustrated in Figure 3, are: (1) **Adaptive Frame-Pruning (AFP)** (pruning) and (2) **Textual Semantic Graph Integration** (compensation).

#### 3.1. Adaptive Frame-Pruning (AFP)

The core of our frame reduction strategy is **AFP**, an algorithm designed to identify and consolidate ‘visual echoes’.

The process involves three key steps: extracting robust fused features, performing adaptive clustering, and selecting a representative frame from each cluster. The entire process is formalized in Algorithm 1.

##### 3.1.1. Fused Feature Extraction.

To ensure that our clustering is sensitive to both low-level visual patterns and high-level semantic content, we employ a fused feature representation. For each keyframe, we extract features from two powerful, pre-trained models: a ResNet-50 [8] backbone, renowned for its strong performance on visual recognition tasks, and a CLIP ViT-B/32 model [25], which excels at aligning images with text and capturing rich semantic meaning. The high-dimensional outputs from both models are passed through separate linear projection layers to map them to a shared 512-dimensional space. The final feature vector  $\mathbf{f}_{\text{fused}}$  for a frame is a weighted combination of the L2-normalized projected features:

$$\mathbf{f}_{\text{fused}} = (1 - \alpha) \cdot \mathbf{f}_{\text{ResNet}} + \alpha \cdot \mathbf{f}_{\text{CLIP}}, \quad (1)$$

where  $\alpha$  is a fusion ratio used to balance the contributions from the visual (ResNet) and semantic (CLIP) features.

##### 3.1.2. Adaptive Hierarchical Clustering.

A key innovation of **AFP** is its ability to adapt the clustering process to the specific content of each video, avoiding a fixed, pre-defined number of clusters. We use Agglomerative Hierarchical Clustering [20], which requires a distance metric and a linkage criterion.

**Distance Metric.** Our distance metric jointly considers visual similarity and temporal proximity. For any two frames  $i$  and  $j$  with fused features  $\mathbf{f}_i, \mathbf{f}_j$  and timestamps  $t_i, t_j$ , the combined distance  $D(i, j)$  is defined as:

$$D(i, j) = \beta \cdot d_{\text{cos}}(\mathbf{f}_i, \mathbf{f}_j) + (1 - \beta) \cdot d_{\text{temp}}(t_i, t_j), \quad (2)$$

where  $d_{\text{cos}}$  is the cosine distance,  $d_{\text{temp}}$  is the normalized absolute difference of timestamps, and  $\beta$  is a weighting factor (set to 0.7). This combined metric ensures that frames that are visually similar but temporally distant are less likely to be clustered together.

**Adaptive Distance Threshold.** Instead of setting a fixed number of clusters, we use a dynamic distance threshold  $\tau$ . This threshold is determined by applying a Gaussian Kernel Density Estimator (KDE) to the distribution of all pairwise visual distances ( $d_{\text{cos}}$ ) within the keyframe set. We identify the peak of this density distribution, which corresponds to the most common distance between frames, and set  $\tau$  slightly above this value. This allows the algorithm to automatically find a natural grouping of frames based on their inherent similarity structure for that specific video.

##### 3.1.3. Representative Frame Selection.

After clustering, a single representative frame must be selected from each resulting cluster. This is a critical step, as

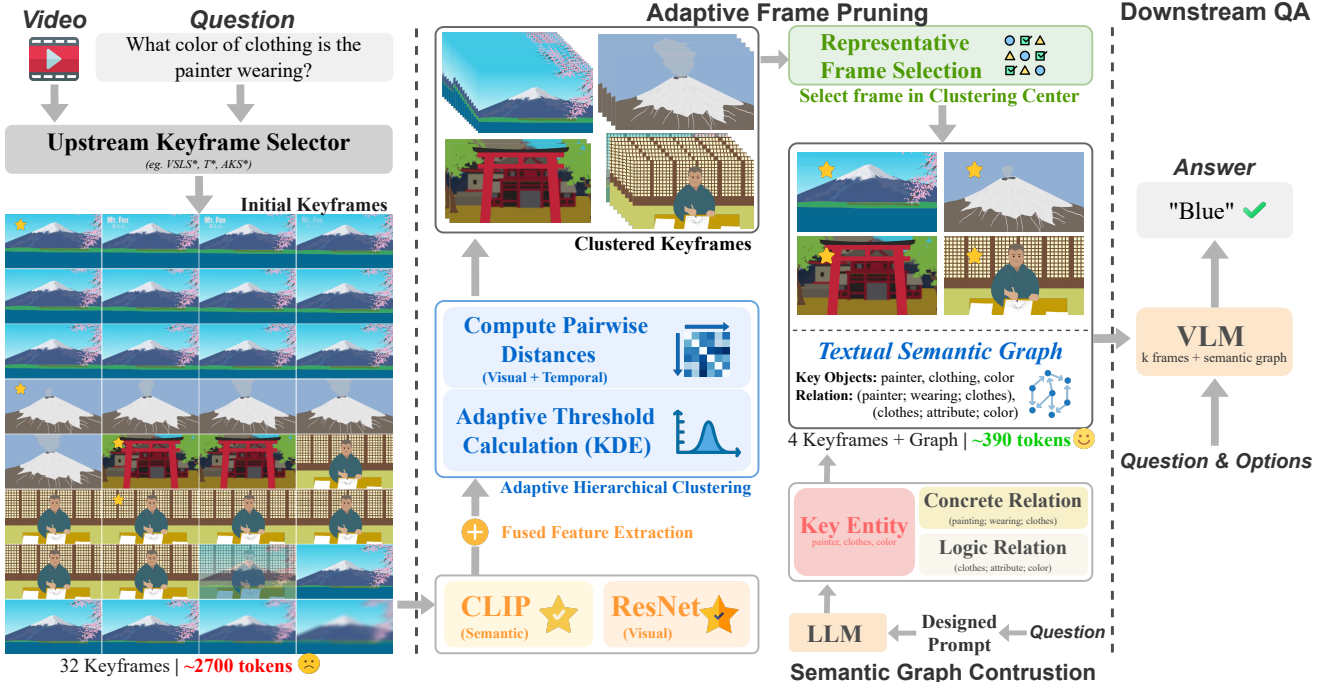


Figure 3. **The Overall Pipeline of Our Proposed Method.** An upstream selector provides initial frames. Our *Adaptive Frame-Pruning (AFP)* module then takes over, performing (1) fused feature extraction and adaptive clustering to produce representative keyframes, and (2) concurrent semantic graph generation. Both are combined into an optimized prompt for the MLLM.

different selection strategies can impact performance. We conducted a detailed ablation study on several strategies (detailed in Appendix F). Our findings show that a **centroid-based selection** approach is the most robust and effective. Therefore, for all our main experiments, we identify the “centroid frame” for each cluster—the one with the minimum average visual feature distance to all other frames within that same cluster. This strategy selects the most visually representative frame, minimizing information loss during pruning without relying on external scores and thus enhancing the generalizability of our *AFP* framework.

### 3.2. Textual Semantic Graph Integration

**Rationale.** The effectiveness of our semantic graph is rooted in principles from context engineering and **Chain-of-Thought (CoT)** prompting [35]. While MLLMs can reason over raw visual inputs, their performance is significantly enhanced when provided with structured, pre-digested context that guides their reasoning process, a core insight from **in-context learning** [3]. Our textualized semantic graph serves precisely this purpose. It acts as a **structured semantic scaffold**, performing two key functions: (1) **Entity Grounding**, by identifying the key objects and actors relevant to the query, and (2) **Relationship Scaffolding**, by providing a high-level summary of the logical and concrete relations between these entities. By injecting this concise,

---

#### Algorithm 1 Adaptive Frame-Pruning (AFP)

**Input:** Initial keyframes  $K = \{k_1, \dots, k_N\}$ , relevance scores  $S = \{s_1, \dots, s_N\}$ , timestamps  $T = \{t_1, \dots, t_N\}$ .  
**Parameters:** Fusion ratio  $\alpha$ , distance weight  $\beta$ .  
**Output:** Refined keyframes  $K'$ .

- 1: Initialize feature set  $F \leftarrow \emptyset$ .
- 2: **for** each keyframe  $k_i \in K$  **do**
- 3:   Extract and project ResNet and CLIP features.
- 4:   Compute  $\mathbf{f}_{\text{fused},i}$  using Eq. 1.
- 5:    $F \leftarrow F \cup \{\mathbf{f}_{\text{fused},i}\}$ .
- 6: **end for**
- 7: Compute pairwise combined distance matrix  $D$  using Eq. 2.
- 8: Compute pairwise visual distances  $D_{\text{cos}}$ .
- 9: Apply KDE to  $D_{\text{cos}}$  to find adaptive threshold  $\tau$ .
- 10: Perform Agglomerative Clustering on  $K$  using distance matrix  $D$  and threshold  $\tau$  to get clusters  $C = \{C_1, \dots, C_M\}$ .
- 11: Initialize refined set  $K' \leftarrow \emptyset$ .
- 12: **for** each cluster  $C_j \in C$  **do**
- 13:   Find  $k^* = \arg \max_{k_i \in C_j} s_i$ .
- 14:    $K' \leftarrow K' \cup \{k^*\}$ .
- 15: **end for**
- 16: **return**  $K'$

---

#### Template for Textualized Semantic Graph

[Here is an additional semantic graph context for this Video-QA]  
Objects in video context: <Objects>  
Relationships between objects: <Relations>

Figure 4. **The template of our textualized semantic graph.** This concise text block, which can be generated, is inserted directly into the downstream Video-QA period as a part of the prompt for MLLM to provide high-level semantic context.

explicit reasoning framework directly into the prompt, we prime the MLLM’s reasoning pathways and focus its attention, enabling it to make more robust inferences from the compact set of visual frames provided by **AFP**. The experimental results in Sec. 5 serve as an empirical validation of this design principle.

**Efficiency Rationale and Token Cost Asymmetry.** A potential concern is that introducing a textual semantic graph might contradict our primary goal of token efficiency. The concern regarding the textual graph’s cost is mitigated by the *asymmetric cost* of tokens: a single image costs 85 tokens [21]. As shown in Figure 5, **AFP** reduces **AKS\*** from 32 frames to 4.1 on average, dropping tokens from **2,877** to **505**. The added semantic graph costs only  $\sim$ 60 tokens, resulting in a final count of **568**. Thus, the visual savings ( $\sim$ 2,300 tokens) vastly outweigh the textual cost, allowing us to trade minimal text tokens for significant performance gains. We “spend” a few dozen text tokens to not only achieve a substantial reduction in visual tokens but, more importantly, to gain a significant performance boost, as validated in our ablation studies (Sec. 5)

**LLM-based Generation for Universal Applicability.** Our framework’s primary and universal strategy for semantic graph construction is a lightweight, LLM-based generation method. This approach ensures our framework’s applicability to *any* keyframe selector, including those that provide no intermediate semantic information (e.g., Uniform Sampling or **AKS**). In this scenario, we prompt a Large Language Model (e.g., GPT-4o) with only the **textual content** of the Video-QA task including question, options. Our carefully designed prompt, detailed in Appendix E, instructs the LLM to act as an “expert visual scene analyst” to infer a wide range of plausible, open-ended relationships. This process is extremely token-efficient as it involves no image inputs.

## 4. Experiments

### 4.1. Experimental Setup

**Datasets and Models.** We evaluate our method on two challenging long-video question-answering benchmarks: **LONG VIDEOBENCH** [41] and **VIDEOMME** [6]. To demonstrate the generalizability, we conduct experiments across three distinct MLLMs: the proprietary **GPT-4o** [10], and two powerful open-source models, **Qwen2.5-VL-7B-Instruct** [2]

and **LLaVA-Video-7B-Qwen2** [13].

**Compared Methods and Baselines.** In our main experiments, we use **AKS\*** as our primary upstream selector to demonstrate the core effectiveness of our method. Our evaluation protocol is designed to rigorously assess our method. For each MLLM, we compare two keyframe sampling strategies in our main results (Table 1):

- **Uniform Sampling:** A naive baseline where a fixed number of frames (32 or 8) are sampled at regular intervals.
- **AKS\*:** Our primary sophisticated baseline. We adapt the state-of-the-art **AKS** [31] framework, which originally uses a dynamic sampling algorithm. To ensure a fair comparison within a fixed budget frame (e.g., exactly 32 or 8 frames), we modify its final step to a Top-K selection based on the relevance scores generated by its BLIP-based model. This adaptation, which we denote as **AKS\***, aligns with the Top-K ablation study presented in the original **AKS** paper and provides a robust, reproducible baseline. A detailed discussion of this modification and a justification for why it does not affect the validity of our ‘visual echoes’ motivation is provided in Appendix D.

- **AFP + Graph:** Our full method, which takes the output of the upstream selector as input and applies our adaptive pruning and semantic graph compensation.

To further validate the generalizability of our approach, we also apply it to two other state-of-the-art selectors, **T\*** and **VSL\***. The results of these extensive generalizability studies are provided in Appendix A and Appendix B.

**Evaluation Metrics.** We evaluate all methods based on three primary criteria:

- **Effectiveness:** We use the official **Accuracy (%)** metric for both benchmarks, calculated via strict exact matching of the predicted option letter against the ground truth, i.e.,  $\text{Accuracy}(\%) = \frac{1}{N} \sum_{i=1}^N \mathbb{1}[\hat{y}_i = y_i] \times 100$ , where  $N$  is the number of questions, and  $\hat{y}_i$  and  $y_i$  are the predicted and ground-truth options.
- **Efficiency:** We measure the **Average Frames** used per query as the efficiency metric, defined as  $\text{AvgFrames} = \frac{1}{N} \sum_{i=1}^N F_i$ , where  $F_i$  is the number of frames used for the  $i$ -th query.
- **Token Efficiency:** We report **estimated token costs** for all methods when paired with GPT-4o. For the  $i$ -th query, the estimated token cost is  $T_i = T_i^{\text{text}} + c_{\text{img}} \cdot F_i$ , where  $T_i^{\text{text}}$  is the token count of the textual prompt (via `tiktoken`),  $F_i$  is the number of low-detail images, and  $c_{\text{img}} = 85$  is the per-image token cost, following OpenAI’s guidelines [21]. We report the average token cost  $\bar{T} = \frac{1}{N} \sum_{i=1}^N T_i$ .

**Implementation and Hyperparameters.** Our framework is implemented in PyTorch. For our main experiments, the core hyperparameters were set to  $\alpha = 0.6$  for the feature fusion ratio and  $\beta = 0.9$  for the distance metric weight. These values were determined through a systematic sensitivity analysis, which revealed a clear cost-utility trade-off, allowing

LONGVIDEOBENCH				VIDEOMME					
Model and Method	Avg. Frames	Video Length Accuracy (%)			Model and Method	Avg. Frames	Video Length Accuracy (%)		
		Long (900-3600s)	Medium (180-600s)	Short (15-60s)			Long (30-60min)	Medium (4-15min)	Short (0-2min)
<i>Evaluation starting from Top 8 Keyframes based on AKS*</i>									
GPT-4o + Uniform	8.0	47.1	49.4	67.3	GPT-4o + Uniform	8.0	<b>54.3</b>	<b>59.3</b>	<b>69.2</b>
GPT-4o + AKS*	8.0	47.0	46.2	66.0	GPT-4o + AKS*	8.0	51.6	52.7	55.8
<b>GPT-4o + <i>AFP+Graph</i></b>	<b>2.1</b>	<b>47.3</b>	<b>53.1</b>	<b>78.0</b>	<b>GPT-4o + <i>AFP+Graph</i></b>	<b>2.2</b>	52.8	55.5	64.4
Qwen2.5-VL-7B + Uniform	8.0	40.3	38.4	42.8	Qwen2.5-VL-7B + Uniform	8.0	36.6	<b>39.1</b>	41.1
Qwen2.5-VL-7B + AKS*	8.0	35.4	41.5	56.0	Qwen2.5-VL-7B + AKS*	8.0	<b>39.4</b>	37.8	42.2
<b>Qwen2.5-VL-7B + <i>AFP+Graph</i></b>	<b>2.1</b>	<b>42.9</b>	<b>46.5</b>	<b>64.0</b>	<b>Qwen2.5-VL-7B + <i>AFP+Graph</i></b>	<b>2.1</b>	37.0	37.1	<b>48.9</b>
LLaVA-Video-7B + Uniform	8.0	40.2	46.9	50.0	LLaVA-Video-7B + Uniform	8.0	37.4	41.1	41.4
LLaVA-Video-7B + AKS*	8.0	41.4	45.8	52.0	LLaVA-Video-7B + AKS*	8.0	38.0	42.2	40.5
LLaVA-Video-7B + <i>AFP+Graph</i>	<b>2.1</b>	<b>44.6</b>	<b>53.1</b>	<b>62.0</b>	LLaVA-Video-7B + <i>AFP+Graph</i>	<b>2.1</b>	<b>43.9</b>	<b>46.0</b>	<b>55.2</b>
<i>Evaluation starting from Top 32 Keyframes based on AKS*</i>									
GPT-4o + Uniform	32.0	<b>50.6</b>	53.5	74.0	GPT-4o + Uniform	32.0	55.2	<b>61.0</b>	<b>71.4</b>
GPT-4o + AKS*	32.0	47.0	49.2	58.0	GPT-4o + AKS*	32.0	<b>55.6</b>	54.5	57.8
<b>GPT-4o + <i>AFP+Graph</i></b>	<b>4.1</b>	49.1	<b>53.5</b>	<b>84.0</b>	<b>GPT-4o + <i>AFP+Graph</i></b>	<b>4.2</b>	55.0	56.7	65.4
Qwen2.5-VL-7B + Uniform	32.0	32.7	36.5	50.0	Qwen2.5-VL-7B + Uniform	32.0	33.6	38.1	<b>60.0</b>
Qwen2.5-VL-7B + AKS*	32.0	35.7	42.7	60.0	Qwen2.5-VL-7B + AKS*	32.0	37.4	39.7	43.8
<b>Qwen2.5-VL-7B + <i>AFP+Graph</i></b>	<b>4.1</b>	<b>43.5</b>	<b>46.9</b>	<b>64.0</b>	<b>Qwen2.5-VL-7B + <i>AFP+Graph</i></b>	<b>4.2</b>	<b>39.2</b>	<b>41.3</b>	50.9
LLaVA-Video-7B + Uniform	32.0	41.7	46.2	40.0	LLaVA-Video-7B + Uniform	32.0	39.1	41.7	39.9
LLaVA-Video-7B + AKS*	32.0	43.5	46.5	50.0	LLaVA-Video-7B + AKS*	32.0	39.6	40.9	41.6
LLaVA-Video-7B + <i>AFP+Graph</i>	<b>4.1</b>	<b>45.2</b>	<b>53.8</b>	<b>64.0</b>	LLaVA-Video-7B + <i>AFP+Graph</i>	<b>4.2</b>	<b>42.6</b>	<b>46.6</b>	<b>53.9</b>

Table 1. **Main Results on LONGVIDEOBENCH and VIDEOMME with different MLLMs.** We compare our full method (*AFP + Graph*) against a sophisticated baseline (*AKS\**) and a naive baseline (Uniform Sampling). Our method achieves superior or highly competitive accuracy while using drastically fewer frames (see Avg. Frames col.). **Bold** indicates the best performing method within each 3-row comparison block for each accuracy column.

our framework to be tuned to prioritize either performance or efficiency. A detailed analysis of these hyperparameters, including a cost-utility trade-off visualization, is provided in Appendix F. Further implementation details and prompt structures are also detailed in the Appendix E.

## 4.2. Main Results and Analysis

Our analysis begins by investigating the “less is more” phenomenon, then presents our main quantitative results, and concludes with a visual analysis of the efficiency-performance trade-off.

**The “Less is More” Paradox and the Brittleness of Advanced Selectors.** Before analyzing our method’s performance, it is crucial to first empirically validate the core challenges our framework is designed to solve. Our experiments reveal a striking finding that underscores the severity of these challenges: the potential **brittleness** of sophisticated selectors when paired with modern MLLMs. For instance, as shown in Table 1, on LONGVIDEOBENCH with GPT-4o (from 8 frames), the advanced *AKS\** selector (47.0% on Long videos) unexpectedly underperforms the naive Uniform Sampling baseline (47.1%). We attribute this performance degradation directly to the core issues formally defined in our introduction: the comprehensive selector, in its effort to maximize recall, inundates the prompt with ‘**visual echoes**’, leading to severe ‘**context dilution**’ that proves detrimental to the MLLM’s advanced reasoning capabilities. This powerful finding confirms that simply adopting a SOTA

selector is not a panacea. Instead, a dedicated **refinement** stage is essential to mitigate these inherent issues and unlock the true potential of query-aware selection.

**Main Quantitative Analysis.** Table 1 presents our main experimental results, comparing our full *AFP + Graph* method against both a naive (Uniform) and a sophisticated (*AKS\**) baseline. The results unequivocally demonstrate the superiority and robustness of our refinement framework.

**Unlocking Performance for Open-Source Models.** The most compelling evidence of our method’s value is its profound impact on open-source models. For instance, using LLaVA-Video-7B on LONGVIDEOBENCH (from 32 frames), our method boosts the accuracy on short videos from 50.0% (*AKS\**) to a remarkable **64.0%**—a **14-point absolute improvement**—while using only an average of 2.1 frames. This significant gain suggests that open-source models are particularly susceptible to context dilution, and our framework is highly effective in providing them with a cleaner, more focused prompt, thereby unlocking their full potential.

**Rescuing and Enhancing State-of-the-Art Selectors.** Our framework not only improves upon but can effectively “rescue” a struggling baseline. Re-examining the LONG VIDEOBENCH GPT-4o (from 8 frames) case, while *AKS\** (46.2%) underperformed Uniform Sampling (49.4%), our *AFP + Graph* applied to *AKS\**’s output achieves **53.1%** on M videos. It successfully closes the performance gap while using **74% fewer frames** (2.1 vs. 8). This demonstrates our method’s power to distill a high-quality signal from a noisy

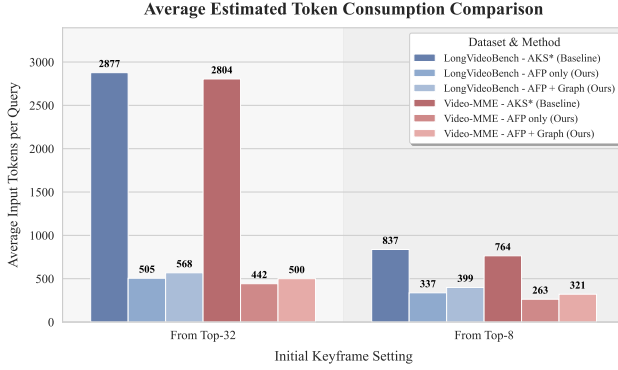


Figure 5. **Average estimated token consumption comparison across datasets and methods.** Token counts are estimated based on OpenAI’s guidelines (see Section 4.1 for details). Our method (***AFP + Graph***) consistently and drastically reduces the token requirements compared to the **AKS\*** baseline across all settings and on both **LONGVIDEOBENCH** and **VIDEOMME** datasets, highlighting its superior and generalizable efficiency.

input.

**Drastic Token Reduction.** This immense efficiency gain is best visualized in Figure 5 and Figure 6. As shown in Figure 5, our approach drastically reduces the estimated token cost across all settings. For example, on **LONG VIDEOBENCH** (from Top-32), the token count plummets from **2,877** with **AKS\*** to just **568** with our method, a reduction of **over 5x**. This makes large-scale Video-QA applications economically viable.

**Visual Analysis of Efficiency and Performance.** Furthermore, the performance-efficiency plot in Figure 6 confirms that our method consistently operates in the highly desirable **top-left quadrant** (high accuracy, low frame usage). The dashed lines (our method) are consistently positioned to the left of and often above the solid lines (the baseline), visually encapsulating our core contribution: achieving a state-of-the-art efficiency-performance trade-off.

## 5. Ablation Studies and Experiment Analysis

To dissect the individual contributions of our core components and validate our framework’s design, we conducted a comprehensive component-wise ablation study. The results, presented in Table 2, compare our full method against a series of carefully designed baselines. Comprehensive results on additional keyframe selectors like **VSL\*** and **T\*** are in Appendix A and Appendix B.

**Ablation Strategies.** To ensure a fair comparison, our ablation study evaluates the following methods, with all visual strategies operating under a **strictly matched frame budget** determined by our **AFP** algorithm’s output count for each Video-QA instance:

- **Text Only (LLM baseline):** Uses only the question and options, establishing a non-visual lower bound.

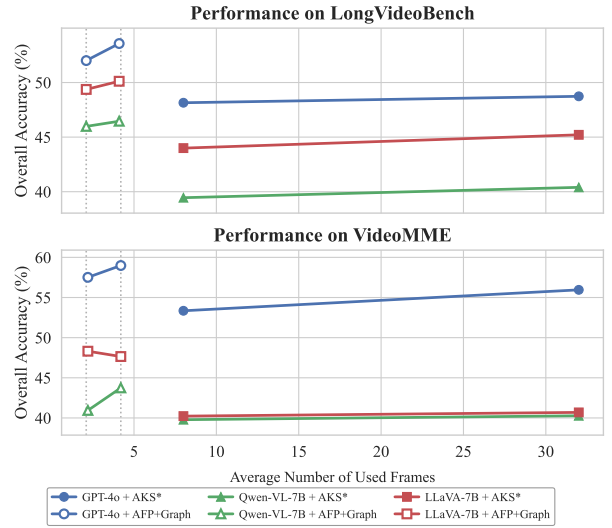


Figure 6. **Efficiency and Performance results of *AFP + Graph* on *AKS\** Keyframes across different MLLMs.** The plot shows the trade-off between overall accuracy and the average number of frames used on both datasets.

- **Graph Only (Ours):** Uses only our textual semantic graph to test its standalone power.
- **Uniform (Matched):** A naive baseline that uniformly samples the matched number of frames.
- **AKS\* (Top- $N$ , Matched):** A strong baseline that truncates the **AKS\***-ranked list to the matched frame count.
- **AFP only (Ours):** Our pruning method without the semantic graph, isolating the effect of intelligent clustering.
- **AFP + Graph (Ours):** Our full, synergistic framework.

**The Power of Semantic Graph.** The most striking result from Table 2 is the immense standalone power of our semantic graph. This jump is vividly illustrated in Figure 7, where the ‘Graph Only’ approach provides a +14.5% absolute accuracy gain over ‘Text Only’ using only a few dozen additional text tokens. This demonstrates that our LLM-based graph construction is a potent form of **knowledge distillation**, effectively converting complex Video-QA problems into more tractable textual reasoning tasks. This remarkable performance of a purely textual graph hints at a promising future: multimodal semantic graph, a concept we explore further.

**The Irreplaceability of Visual Grounding.** While the graph excels at abstract reasoning, the results prove that visual evidence is irreplaceable. In every experimental group in Table 2, ***AFP + Graph*** consistently outperforms the high-performing ‘Graph Only’ baseline. For example, on **LONG VIDEOBENCH** (Short) using Qwen2.5-VL-7B where ‘Graph Only’ achieves a remarkable 56.0%, adding just 2.1 frames boosts the accuracy further to **64.0%**. Figure 7 reinforces this principle, showing our full framework (***AFP + Graph***) achieving the peak accuracy, surpassing all other variants. This confirms our central thesis: the semantic graph pro-

Method	Avg. Fr.	Avg. Tok.	Long(%)	Med.(%)	Short(%)
<i>Ablation from AKS* Top 32 Keyframes (Model: GPT-4o)</i>					
Text Only	0.0	157.05	42.9	45.8	48.0
Graph Only	0.0	219.48	47.0	53.5	82.0
Uniform (M)	4.1	505.21	47.0	47.7	66.0
AKS* (Top-N, M)	4.1	505.21	43.5	45.8	62.0
<b>AFP only</b>	4.1	505.21	47.9	45.8	64.0
<b>AFP + Graph</b>	<b>4.1</b>	<b>56.74</b>	<b>49.1</b>	<b>53.5</b>	<b>84.0</b>
<i>Ablation from AKS* Top 8 Keyframes (Model: Qwen2.5-VL-7B)</i>					
Text Only	0.0	N/A	35.1	38.1	52.0
Graph Only	0.0	N/A	37.5	41.2	56.0
Uniform (M)	2.1	N/A	39.0	38.8	62.0
AKS* (Top-N, M)	2.1	N/A	41.4	41.5	56.0
<b>AFP only</b>	2.1	N/A	41.4	42.3	60.0
<b>AFP + Graph</b>	<b>2.1</b>	N/A	<b>42.9</b>	<b>46.5</b>	<b>64.0</b>

(a) Results on the LONGVIDEOBENCH dataset.

Method	Avg. Fr.	Avg. Tok.	Long(%)	Med.(%)	Short(%)
<i>Ablation from AKS* Top 32 Keyframes (Model: GPT-4o)</i>					
Text Only	0.0	84.10	43.9	42.7	35.4
Graph Only	0.0	141.52	51.1	54.3	60.4
Uniform (M)	4.2	442.18	53.1	53.3	59.2
AKS* (Top-N, M)	4.2	442.18	51.1	50.0	53.2
<b>AFP only</b>	4.2	442.18	53.7	51.6	57.1
<b>AFP + Graph</b>	<b>4.2</b>	<b>499.60</b>	<b>55.0</b>	<b>56.7</b>	<b>65.4</b>
<i>Ablation from AKS* Top 8 Keyframes (Model: LLaVA-Video-7B)</i>					
Text Only	0.0	N/A	37.4	40.4	41.6
Graph Only	0.0	N/A	42.3	46.0	54.2
Uniform (M)	2.1	N/A	39.2	40.6	39.7
AKS* (Top-N, M)	2.1	N/A	37.8	40.8	41.1
<b>AFP only</b>	2.1	N/A	40.6	40.7	40.7
<b>AFP + Graph</b>	<b>2.1</b>	N/A	<b>43.9</b>	<b>46.0</b>	<b>55.2</b>

(b) Results on the VIDEOMME dataset.

Table 2. **Comprehensive component-wise ablation study under a matched frame budget.** We compare our full method against baselines including text-only, graph-only, uniform sampling, and AKS\* truncation. Our full method consistently outperforms all others. Token counts are estimated as detailed in Section 4.1.

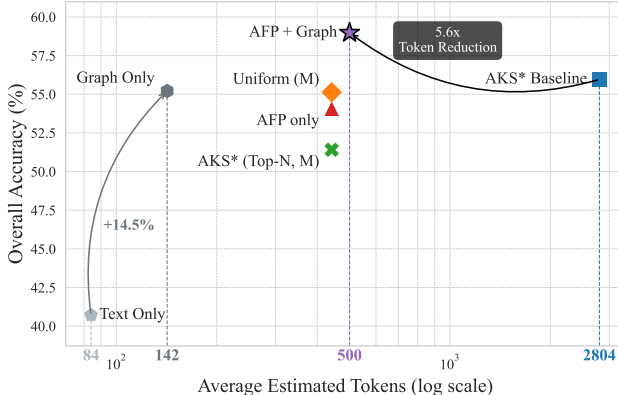


Figure 7. **Efficiency-Performance Trade-off Analysis.** This scatter plot visualizes the results from our ablation study on VIDEOMME based on the AKS\* Top-32 setting with GPT-4o (detailed in Table 2). The x-axis represents the average token cost (log scale), while the y-axis shows overall QA accuracy. Our full framework, **AFP + Graph**, resides in the optimal top-left quadrant, achieving the highest accuracy with a 5.6x token reduction compared to the AKS\* baseline. This visually encapsulates our “Less is More” contribution: achieving superior performance with significantly greater efficiency.

vides a powerful reasoning scaffold, but the concise visual evidence selected by **AFP** is essential for grounding that reasoning and achieving peak performance.

**“Less is More” Principle.** When focusing on frame-based strategies, the superiority of **AFP** is clear. For GPT-4o on LONGVIDEOBENCH, Table 2 shows that ‘**AFP only**’ (47.9% on Long videos) outperforms both ‘Uniform (Matched)’ (47.0%) and the sophisticated ‘AKS\* (Top-N, Matched)’ baseline (43.5%). The overall synergistic advantage of our framework is best encapsulated in Figure 7. Our full **AFP +**

**Graph** method orchestrates a dramatic shift from the high-cost, moderate-performance regime of the ‘AKS\* Baseline’ to the highly desirable top-left quadrant. It not only achieves the highest overall accuracy but does so with a staggering **5.6x** reduction in token cost. This visually validates our core claim: our framework successfully refines a verbose, noisy prompt into one that is both token-efficient and semantically potent, thereby perfectly embodying the core “**Less is More**” principle in practice.

## 6. Conclusion

In this work, we tackled the challenge of high token usage in MLLM-based Video-QA, following the idea that fewer but more informative frames can support stronger reasoning. We proposed a two-part framework based on **Adaptive Frame-Pruning (AFP)** and a **text-based semantic graph**. Our experiments showed that this design reduces both frame count and token count while also improving QA accuracy by limiting context noise. We further introduced the concept of ‘**visual echoes**’, a challenge that arises from temporal redundancy in videos, and provided a clear way to handle it through selective filtering and prompt refinement. Together, these contributions demonstrate that efficient input design can yield practical benefits for Video-QA systems.

Looking ahead, we see opportunities to extend our approach beyond a text-based graph toward a ‘**Multimodal Semantic Graph**’ that integrates audio cues, motion patterns, and trajectories. Such a graph could act as a compact and informative summary of long videos, addressing the global-feature limits highlighted in our failure case analysis (Appendix G). We expect more stable reasoning over long sequences while keeping token usage low.

## References

[1] Jinze Bai, Shuai Bai, Shusheng Yang, Shijie Wang, Sinan Tan, Peng Wang, Junyang Lin, Chang Zhou, and Jingren Zhou. Qwen-vl: A versatile vision-language model for understanding, localization, text reading, and beyond. *arXiv preprint arXiv:2308.12966*, 2023. 2

[2] Shuai Bai, Kejin Chen, Xuejing Liu, Jialin Wang, Wenbin Ge, Sibo Song, Kai Dang, Peng Wang, Shijie Wang, Jun Tang, et al. Qwen2. 5-vl technical report. *arXiv preprint arXiv:2502.13923*, 2025. 5

[3] Tom Brown, Benjamin Mann, Nick Ryder, Melanie Subbiah, Jared D Kaplan, Prafulla Dhariwal, Arvind Neelakantan, Pranav Shyam, Girish Sastry, Amanda Askell, et al. Language models are few-shot learners. *Advances in neural information processing systems*, 33:1877–1901, 2020. 4

[4] Zesen Cheng, Sicong Leng, Hang Zhang, Yifei Xin, Xin Li, Guanzheng Chen, Yongxin Zhu, Wenqi Zhang, Ziyang Luo, Deli Zhao, and Li Bing. Videollama 2: Advancing spatial-temporal modeling and audio understanding in video-llms. *ArXiv*, abs/2406.07476, 2024. 2

[5] Yue Fan, Xiaojian Ma, Ruijie Wu, Yuntao Du, Jiaqi Li, Zhi Gao, and Qing Li. Videoagent: A memory-augmented multimodal agent for video understanding. In *European Conference on Computer Vision*, pages 75–92. Springer, 2024. 3

[6] Chaoyou Fu, Yuhua Dai, Yondong Luo, Lei Li, Shuhuai Ren, Renrui Zhang, Zihan Wang, Chenyu Zhou, Yunhang Shen, Mengdan Zhang, Peixian Chen, Yanwei Li, Shaohui Lin, Sirui Zhao, Ke Li, Tong Xu, Xiawu Zheng, Enhong Chen, Rongrong Ji, and Xing Sun. Video-mme: The first-ever comprehensive evaluation benchmark of multi-modal llms in video analysis. *ArXiv*, abs/2405.21075, 2024. 5

[7] Weiyu Guo, Ziyang Chen, Shaoguang Wang, Jianxiang He, Yijie Xu, Jinhui Ye, Ying Sun, and Hui Xiong. Logic-in-frames: Dynamic keyframe search via visual semantic-logical verification for long video understanding. *arXiv preprint arXiv:2503.13139*, 2025. 3, 1

[8] Kaiming He, Xiangyu Zhang, Shaoqing Ren, and Jian Sun. Deep residual learning for image recognition. In *Proceedings of the IEEE conference on computer vision and pattern recognition*, pages 770–778, 2016. 3

[9] Bin Huang, Xin Wang, Hong Chen, Zihan Song, and Wenwu Zhu. Vtimellm: Empower llm to grasp video moments. *2024 IEEE/CVF Conference on Computer Vision and Pattern Recognition (CVPR)*, pages 14271–14280, 2023. 2

[10] Aaron Hurst, Adam Lerer, Adam P Goucher, Adam Perelman, Aditya Ramesh, Aidan Clark, AJ Ostrow, Akila Welihinda, Alan Hayes, Alec Radford, et al. Gpt-4o system card. *arXiv preprint arXiv:2410.21276*, 2024. 1, 2, 5

[11] Peng Jin, Ryuichi Takanobu, Wancai Zhang, Xiaochun Cao, and Li Yuan. Chat-univi: Unified visual representation empowers large language models with image and video understanding. In *Proceedings of the IEEE/CVF Conference on Computer Vision and Pattern Recognition*, pages 13700–13710, 2024. 3

[12] Ranjay Krishna, Yuke Zhu, Oliver Groth, Justin Johnson, Kenji Hata, Joshua Kravitz, Stephanie Chen, Yannis Kalanidis, Li-Jia Li, David A Shamma, et al. Visual genome: Connecting language and vision using crowdsourced dense image annotations. *International journal of computer vision*, 123(1):32–73, 2017. 3

[13] Feng Li, Renrui Zhang, Hao Zhang, Yuanhan Zhang, Bo Li, Wei Li, Zejun Ma, and Chunyuan Li. Llava-next-interleave: Tackling multi-image, video, and 3d in large multimodal models. *arXiv preprint arXiv:2407.07895*, 2024. 5

[14] KunChang Li, Yinan He, Yi Wang, Yizhuo Li, Wenhai Wang, Ping Luo, Yali Wang, Limin Wang, and Yu Qiao. Videochat: Chat-centric video understanding. *arXiv preprint arXiv:2305.06355*, 2023. 3

[15] Hao Liang, Jiapeng Li, Tianyi Bai, Xijie Huang, Linzhuang Sun, Zhengren Wang, Conghui He, Bin Cui, Chong Chen, and Wentao Zhang. Keyvideollm: Towards large-scale video keyframe selection. *arXiv preprint arXiv:2407.03104*, 2024. 3

[16] Bin Lin, Yang Ye, Bin Zhu, Jiaxi Cui, Munan Ning, Peng Jin, and Li Yuan. Video-llava: Learning united visual representation by alignment before projection. *arXiv preprint arXiv:2311.10122*, 2023. 1, 2

[17] Ruiyu Luo, Ziwang Zhao, Min Yang, Junwei Dong, Da Li, Pengcheng Lu, Tao Wang, Linmei Hu, Minghui Qiu, and Zhongyu Wei. Valley: Video assistant with large language model enhanced ability. *arXiv preprint arXiv:2306.07207*, 2023. 2

[18] Ziyu Ma, Chenhui Gou, Hengcan Shi, Bin Sun, Shutao Li, Hamid Rezatofighi, and Jianfei Cai. Drvideo: Document retrieval based long video understanding. In *Proceedings of the Computer Vision and Pattern Recognition Conference*, pages 18936–18946, 2025. 2

[19] Muhammad Maaz, Hanoona Rasheed, Salman Khan, and Fahad Shahbaz Khan. Video-chatgpt: Towards detailed video understanding via large vision and language models. *arXiv preprint arXiv:2306.05424*, 2023. 1, 2

[20] Fionn Murtagh and Pedro Contreras. Algorithms for hierarchical clustering: an overview. *Wiley interdisciplinary reviews: data mining and knowledge discovery*, 2(1):86–97, 2012. 3

[21] OpenAI. Vision - API docs. <https://platform.openai.com/docs/guides/vision>, 2024. Accessed: Oct 28, 2025]. 5

[22] Jongwoo Park, Kanchana Ranasinghe, Kumara Kahatapitiya, Wonjeong Ryu, Donghyun Kim, and Michael S Ryoo. Too many frames, not all useful: Efficient strategies for long-form video qa. *arXiv preprint arXiv:2406.09396*, 2024. 3

[23] Adam Paszke, Sam Gross, Francisco Massa, Adam Lerer, James Bradbury, Gregory Chanan, Trevor Killeen, Zeming Lin, Natalia Gimelshein, Luca Antiga, Alban Desmaison, Andreas Kopf, Edward Yang, Zachary DeVito, Martin Raison, Alykhan Tejani, Sasank Chilamkurthy, Benoit Steiner, Lu Fang, Junjie Bai, and Soumith Chintala. Pytorch: An imperative style, high-performance deep learning library. In *Advances in Neural Information Processing Systems 32*, pages 8024–8035. Curran Associates, Inc., 2019. 5

[24] F. Pedregosa, G. Varoquaux, A. Gramfort, V. Michel, B. Thirion, O. Grisel, M. Blondel, P. Prettenhofer, R. Weiss, V. Dubourg, J. Vanderplas, A. Passos, D. Cournapeau, M.

Brucher, M. Perrot, and E. Duchesnay. Scikit-learn: Machine learning in Python. *Journal of Machine Learning Research*, 12:2825–2830, 2011. 5

[25] Alec Radford, Jong Wook Kim, Chris Hallacy, Aditya Ramesh, Gabriel Goh, Sandhini Agarwal, Girish Sastry, Amanda Askell, Pamela Mishkin, Jack Clark, et al. Learning transferable visual models from natural language supervision. In *International conference on machine learning*, pages 8748–8763. PMLR, 2021. 3

[26] Shuhuai Ren, Linli Yao, Shicheng Li, Xu Sun, and Lu Hou. Timechat: A time-sensitive multimodal large language model for long video understanding. In *Proceedings of the IEEE/CVF Conference on Computer Vision and Pattern Recognition*, pages 14313–14323, 2024. 2

[27] David Romero and Thamar Solorio. Question-instructed visual descriptions for zero-shot video question answering. *arXiv preprint arXiv:2402.10698*, 2024. 3

[28] Dingjie Song, Wenjun Wang, Shunian Chen, Xidong Wang, Michael Guan, and Benyou Wang. Less is more: A simple yet effective token reduction method for efficient multi-modal llms. *arXiv preprint arXiv:2409.10994*, 2024. 3

[29] Enxin Song, Wenhao Chai, Guanhong Wang, Yucheng Zhang, Haoyang Zhou, Feiyang Wu, Haozhe Chi, Xun Guo, Tian Ye, Yanting Zhang, et al. Moviechat: From dense token to sparse memory for long video understanding. In *Proceedings of the IEEE/CVF Conference on Computer Vision and Pattern Recognition*, pages 18221–18232, 2024. 1, 2

[30] D’idac Sur’is, Sachit Menon, and Carl Vondrick. Vipergrpt: Visual inference via python execution for reasoning. *2023 IEEE/CVF International Conference on Computer Vision (ICCV)*, pages 11854–11864, 2023. 2

[31] Xi Tang, Jihao Qiu, Lingxi Xie, Yunjie Tian, Jianbin Jiao, and Qixiang Ye. Adaptive keyframe sampling for long video understanding. In *Proceedings of the Computer Vision and Pattern Recognition Conference*, pages 29118–29128, 2025. 3, 5, 4

[32] Gemini Team, Rohan Anil, Sebastian Borgeaud, Jean-Baptiste Alayrac, Jiahui Yu, Radu Soricut, Johan Schalkwyk, Andrew M Dai, Anja Hauth, Katie Millican, et al. Gemini: a family of highly capable multimodal models. *arXiv preprint arXiv:2312.11805*, 2023. 1, 2

[33] Xiaohan Wang, Yuhui Zhang, Orr Zohar, and Serena Yeung-Levy. Videoagent: Long-form video understanding with large language model as agent. *ArXiv*, abs/2403.10517, 2024. 2, 3

[34] Ziyang Wang, Shoubin Yu, Elias Stengel-Eskin, Jaehong Yoon, Feng Cheng, Gedas Bertasius, and Mohit Bansal. Videotree: Adaptive tree-based video representation for llm reasoning on long videos. In *Proceedings of the Computer Vision and Pattern Recognition Conference*, pages 3272–3283, 2025. 3

[35] Jason Wei, Xuezhi Wang, Dale Schuurmans, Maarten Bosma, Fei Xia, Ed Chi, Quoc V Le, Denny Zhou, et al. Chain-of-thought prompting elicits reasoning in large language models. *Advances in neural information processing systems*, 35:24824–24837, 2022. 4

[36] Yuetian Weng, Mingfei Han, Haoyu He, Xiaojun Chang, and Bohan Zhuang. Longvlm: Efficient long video understanding via large language models. In *European Conference on Computer Vision*, pages 453–470. Springer, 2024. 2

[37] Chenfei Wu, Shengming Yin, Weizhen Qi, Xiaodong Wang, Zecheng Tang, and Nan Duan. Visual chatgpt: Talking, drawing and editing with visual foundation models. *arXiv preprint arXiv:2303.04671*, 2023. 2

[38] Zuxuan Wu, Caiming Xiong, Chih-Yao Ma, Richard Socher, and Larry S Davis. Adaframe: Adaptive frame selection for fast video recognition. In *Proceedings of the IEEE/CVF Conference on Computer Vision and Pattern Recognition*, pages 1278–1287, 2019. 3

[39] Zonghan Wu, Shirui Pan, Fengwen Chen, Guodong Long, Chengqi Zhang, and Philip S Yu. A comprehensive survey on graph neural networks. *IEEE transactions on neural networks and learning systems*, 32(1):4–24, 2020. 3

[40] Antoine Yang, Arsha Nagrani, Paul Hongsuck Seo, Antoine Miech, Jordi Pont-Tuset, Ivan Laptev, Josef Sivic, and Cordelia Schmid. Vid2seq: Large-scale pretraining of a visual language model for dense video captioning. *2023 IEEE/CVF Conference on Computer Vision and Pattern Recognition (CVPR)*, pages 10714–10726, 2023. 2

[41] Jinhui Ye, Zihan Wang, and Haosen Sun. Longvideo-haystack. <https://huggingface.co/datasets/LVHaystack/LongVideoHaystack>, 2025. v1.0. 5

[42] Jinhui Ye, Zihan Wang, Haosen Sun, Keshigeyan Chandrasegaran, Zane Durante, Cristobal Eyzaguirre, Yonatan Bisk, Juan Carlos Niebles, Ehsan Adeli, Li Fei-Fei, et al. Rethinking temporal search for long-form video understanding. In *Proceedings of the Computer Vision and Pattern Recognition Conference*, pages 8579–8591, 2025. 3, 2

[43] Shoubin Yu, Jaemin Cho, Prateek Yadav, and Mohit Bansal. Self-chained image-language model for video localization and question answering. *Advances in Neural Information Processing Systems*, 36:76749–76771, 2023. 3

[44] Ce Zhang, Taixi Lu, Md Mohaiminul Islam, Ziyang Wang, Shoubin Yu, Mohit Bansal, and Gedas Bertasius. A simple llm framework for long-range video question-answering. In *Proceedings of the 2024 Conference on Empirical Methods in Natural Language Processing*, pages 21715–21737, 2024. 3

[45] Hang Zhang, Xin Li, and Lidong Bing. Video-llama: An instruction-tuned audio-visual language model for video understanding. *arXiv preprint arXiv:2306.02858*, 2023. 2

[46] Siwei Zhang, Yun Xiong, Yateng Tang, Xi Chen, Zian Jia, Zehao Gu, Jiarong Xu, and Jiawei Zhang. Unifying text semantics and graph structures for temporal text-attributed graphs with large language models. *ArXiv*, abs/2503.14411, 2025. 3

[47] Yue Zhao, Ishan Misra, Philipp Krähenbühl, and Rohit Girdhar. Learning video representations from large language models. *2023 IEEE/CVF Conference on Computer Vision and Pattern Recognition (CVPR)*, pages 6586–6597, 2022. 2

[48] Yue Zhao, Ishan Misra, Philipp Krähenbühl, and Rohit Girdhar. Learning video representations from large language models. In *Proceedings of the IEEE/CVF Conference on Computer Vision and Pattern Recognition*, pages 6586–6597, 2023. 2

# Less is More: Token-Efficient Video-QA via Adaptive Frame-Pruning and Semantic Graph Integration

## Supplementary Material

### A. Generalizability Studies on VSLS\*

**A Note on VSLS\*.** In our generalizability study, we use a specific, publicly available version of the VSLS codebase from May 2025, which we denote as *VSLS\**. It is important to note that this version differs slightly from the final published version of *VSLS* [7]. The primary difference lies in the sampling strategy: this earlier version normalizes the relevance scores into a probability distribution before sampling, whereas the final version performs a direct Top-K selection on the raw scores. We use this specific, frozen version to ensure the reproducibility of our experiments presented here.

**Experimental Setup.** This section provides the complete component-wise ablation results for applying our framework to the output of *VSLS\**.

The methods compared are:

- **VSLS\* Baseline:** The two high-cost methods using a fixed number of frames (32 or 8) via ‘*VSLS\**’.
- **Matched-Budget Strategies:** Four low-cost methods that all operate on the same, drastically reduced number of frames determined by our *AFP* algorithm for each Video-QA instance.
  - Uniform (Matched): Naive uniform sampling.
  - *VSLS\** (Top-N, Matched): A strong baseline that truncates the *VSLS\** list.
  - *AFP* only (Ours): Our pruning method without the graph.
  - *AFP + Graph* (Ours): Our full proposed method.

The detailed results are presented in Table 3.

**Analysis from Tabular Data.** The results in Table 3 robustly confirm that our framework acts as a versatile refinement module for *VSLS\**. First, our full *AFP + Graph* method achieves a highly favorable efficiency-performance trade-off. The performance gains are particularly striking on open-source models. For instance, on **LONGVIDEOBENCH** with LLaVA-Video-7B (from 8 frames), our method boosts the accuracy on short videos from 50.0% (*VSLS\** Baseline) to a remarkable **72.0%**—a **+22 point** absolute improvement—while using only 2.2 frames. Second, the superiority of our frame selection is evident. Under a strictly matched frame budget, ‘*AFP* only’ (e.g., on **VIDEOMME** with GPT-4o from 32 frames) demonstrates clear performance advantages over ‘*VSLS\** (Top-N, Matched)’, indicating that our intelligent clustering selects a more representative set of frames. In addition, the semantic graph proves its crucial

role. The consistent and significant performance leap from ‘*AFP* only’ to ‘*AFP + Graph*’ across all settings validates our rationale that the graph provides the essential semantic scaffolding to unlock the MLLM’s full potential.

**Visual Analysis of Efficiency-Performance.** This trade-off is best visualized in the efficiency-performance plot in Figure 8, which focuses on the challenging **GPT-4o on VIDEOMME (from Top-32)** scenario. The plot clearly illustrates *AFP + Graph*’s superiority. The *VSLS\** Baseline resides in the bottom-right, representing high cost and moderate performance. Within the highly competitive low-cost zone on the left, our full *AFP + Graph* method distinguishes itself, positioned highest in the desirable top-left quadrant. It not only significantly outperforms the ‘*VSLS\** (Top-N, Matched)’ baseline (57.55% vs. 51.29%) but also surpasses the ‘*AFP* only’ approach (54.18%), demonstrating the crucial performance boost provided by the semantic graph.

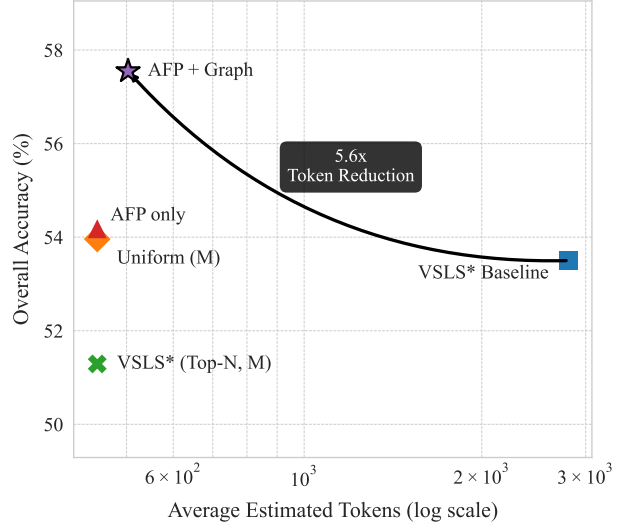


Figure 8. **Efficiency-Performance Trade-off on VIDEOMME with VSLS\*.** This plot visualizes the results for GPT-4o when refining the Top-32 output from *VSLS\**. The x-axis (log scale) represents token cost, and the y-axis represents weighted average accuracy. The top-left region is optimal.

### B. Generalizability Studies on $T^*$

**Experimental Setup.** To further validate the universal applicability of our framework, we conducted a comprehensive set of experiments applying it to another state-of-the-art

Method	Avg. Fr.	Long(%)	Med.(%)	Short(%)
<i>Evaluation from Top 8 Keyframes</i>				
<b>Model: GPT-4o</b>				
VSLS* Baseline	8.0	44.6	46.9	66.0
Uniform (Matched)	2.2	47.6	48.1	62.0
VSLS* (Top-N, Matched)	2.2	<b>50.3</b>	48.1	66.0
<i>AFP</i> only (Ours)	2.2	45.5	51.5	56.0
<i>AFP + Graph</i> (Ours)	<b>2.2</b>	47.3	<b>53.5</b>	<b>84.0</b>
<b>Model: Qwen2.5-VL-7B-Instruct</b>				
VSLS* Baseline	8.0	<b>45.8</b>	<b>49.2</b>	54.0
Uniform (Matched)	2.2	38.1	41.9	<b>70.0</b>
VSLS* (Top-N, Matched)	2.2	44.0	47.3	56.0
<i>AFP</i> only (Ours)	2.2	40.2	45.0	68.0
<i>AFP + Graph</i> (Ours)	<b>2.2</b>	42.6	45.4	62.0
<b>Model: LLaVA-Video-7B-Qwen2</b>				
VSLS* Baseline	8.0	42.6	43.5	50.0
Uniform (Matched)	2.2	39.3	46.2	42.0
VSLS* (Top-N, Matched)	2.2	40.5	42.7	46.0
<i>AFP</i> only (Ours)	2.2	41.1	44.6	44.0
<i>AFP + Graph</i> (Ours)	<b>2.2</b>	<b>45.5</b>	<b>49.6</b>	<b>72.0</b>
<i>Evaluation from Top 32 Keyframes</i>				
<b>Model: GPT-4o</b>				
VSLS* Baseline	32.0	46.1	45.0	76.0
Uniform (Matched)	4.2	47.9	48.8	64.0
VSLS* (Top-N, Matched)	4.2	<b>50.9</b>	<b>53.8</b>	64.0
<i>AFP</i> only (Ours)	4.2	45.5	47.7	66.0
<i>AFP + Graph</i> (Ours)	<b>4.2</b>	49.4	51.5	<b>80.0</b>
<b>Model: Qwen2.5-VL-7B-Instruct</b>				
VSLS* Baseline	32.0	38.7	42.3	54.0
Uniform (Matched)	4.2	45.8	45.0	68.0
VSLS* (Top-N, Matched)	4.2	<b>50.3</b>	<b>53.1</b>	66.0
<i>AFP</i> only (Ours)	4.2	40.2	41.9	60.0
<i>AFP + Graph</i> (Ours)	<b>4.2</b>	42.9	46.9	<b>66.0</b>
<b>Model: LLaVA-Video-7B-Qwen2</b>				
VSLS* Baseline	32.0	41.7	48.1	54.0
Uniform (Matched)	4.2	38.1	47.3	52.0
VSLS* (Top-N, Matched)	4.2	40.2	45.8	52.0
<i>AFP</i> only (Ours)	4.2	41.7	43.5	50.0
<i>AFP + Graph</i> (Ours)	<b>4.2</b>	<b>45.2</b>	<b>50.0</b>	<b>62.0</b>

(a) Results on the LONGVIDEOBENCH dataset.

Method	Avg. Fr.	Long(%)	Med.(%)	Short(%)
<i>Evaluation from Top 8 Keyframes</i>				
<b>Model: GPT-4o</b>				
VSLS* Baseline	8.0	51.7	52.4	56.5
Uniform (Matched)	2.1	52.4	53.4	58.6
VSLS* (Top-N, Matched)	2.1	50.5	49.8	56.0
<i>AFP</i> only (Ours)	2.1	53.1	51.8	57.3
<i>AFP + Graph</i> (Ours)	<b>2.1</b>	<b>53.5</b>	<b>56.5</b>	<b>63.8</b>
<b>Model: Qwen2.5-VL-7B-Instruct</b>				
VSLS* Baseline	8.0	36.6	39.1	41.1
Uniform (Matched)	2.1	38.5	40.2	42.9
VSLS* (Top-N, Matched)	2.1	38.1	37.9	41.4
<i>AFP</i> only (Ours)	2.1	39.2	38.8	42.4
<i>AFP + Graph</i> (Ours)	<b>2.1</b>	<b>38.1</b>	<b>40.2</b>	<b>50.1</b>
<b>Model: LLaVA-Video-7B-Qwen2</b>				
VSLS* Baseline	8.0	38.7	41.5	41.3
Uniform (Matched)	2.1	40.6	41.2	38.3
VSLS* (Top-N, Matched)	2.1	39.2	40.2	38.5
<i>AFP</i> only (Ours)	2.1	38.9	41.0	40.3
<i>AFP + Graph</i> (Ours)	<b>2.1</b>	<b>44.2</b>	<b>47.9</b>	<b>54.5</b>
<i>Evaluation from Top 32 Keyframes</i>				
<b>Model: GPT-4o</b>				
VSLS* Baseline	32.0	51.7	52.4	56.5
Uniform (Matched)	4.3	52.3	52.6	57.1
VSLS* (Top-N, Matched)	4.3	49.7	50.2	54.1
<i>AFP</i> only (Ours)	4.3	52.5	52.5	57.7
<i>AFP + Graph</i> (Ours)	<b>4.3</b>	<b>53.0</b>	<b>56.4</b>	<b>63.4</b>
<b>Model: Qwen2.5-VL-7B-Instruct</b>				
VSLS* Baseline	32.0	37.9	39.1	<b>55.8</b>
Uniform (Matched)	4.3	39.1	43.5	43.6
VSLS* (Top-N, Matched)	4.3	37.9	40.2	42.5
<i>AFP</i> only (Ours)	4.3	38.3	39.8	42.5
<i>AFP + Graph</i> (Ours)	<b>4.3</b>	<b>39.9</b>	<b>44.0</b>	51.8
<b>Model: LLaVA-Video-7B-Qwen2</b>				
VSLS* Baseline	32.0	37.4	40.6	42.1
Uniform (Matched)	4.3	39.6	40.6	41.7
VSLS* (Top-N, Matched)	4.3	38.1	41.1	41.2
<i>AFP</i> only (Ours)	4.3	39.8	40.9	41.5
<i>AFP + Graph</i> (Ours)	<b>4.3</b>	<b>43.8</b>	<b>47.9</b>	<b>56.7</b>

(b) Results on the VIDEOMME dataset.

Table 3. **Complete component-wise ablation study results on the LONGVIDEOBENCH and VIDEOMME datasets using VSLS\* as the upstream selector.** For each model and initial frame setting, we compare our full method against various baselines. **Bold** indicates the best performance among the four matched-budget strategies for each accuracy column.

keyframe selector,  $T^*$  [42]. The comparison follows the same structure as our VSLS\* study, with detailed results presented in Table 4.

**Analysis from Tabular Data.** The results in Table 4 further solidify our framework’s universal applicability. **First**, our full method consistently offers a superior cost-utility trade-off, with gains being most pronounced on open-source models. For instance, when refining the  $T^*$  output for LLaVA-Video-7B on VIDEOMME (from 32 frames), our method elevates the accuracy on short videos from 41.6% to **55.0%**—a **+13.4 point** improvement. **Second**, the quality of frames selected by ‘*AFP* only’ is demonstrably high.

Under the matched-budget setting for GPT-4o on LONG VIDEOBENCH (from 8 frames), ‘*AFP* only’ (47.3% on Long videos) outperforms both ‘Uniform (Matched)’ (45.5%) and ‘ $T^*$  (Top-N, Matched)’ (46.4%). **Finally**, the semantic graph consistently provides a significant performance boost, reinforcing our central thesis about the synergy between our two components.

**Visual Analysis of Efficiency-Performance.** This trade-off is powerfully visualized in the efficiency-performance plot in Figure 9, which highlights the **GPT-4o on VIDEOMME (from Top-32)** scenario. Similar to the VSLS\* case, the  $T^*$  Baseline resides in the high-cost, bottom-right

region. Within the highly competitive low-cost zone, our full **AFP + Graph** method once again establishes itself as the superior choice, occupying the highest point in the desirable top-left quadrant. It significantly outperforms the ‘ $T^*$  (Top-N, Matched)’ baseline (56.91% vs. 51.20%) and shows a clear improvement over the ‘**AFP only**’ approach (53.66%). This parallel success story proves that our framework’s effectiveness is not tied to a specific selector but stems from its fundamental principles of intelligent pruning and semantic compensation.

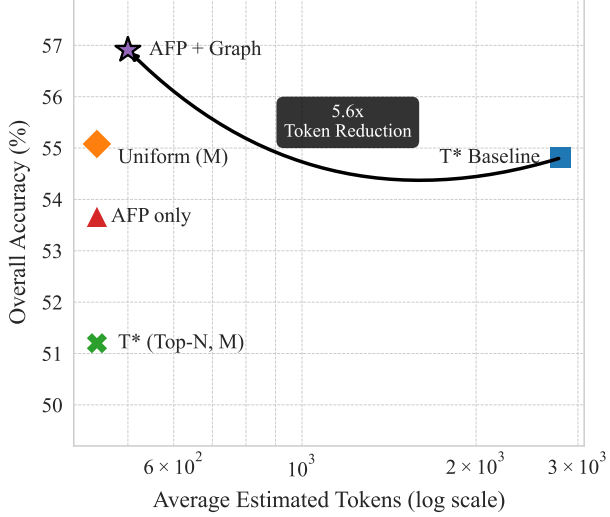


Figure 9. **Efficiency-Performance Trade-off on VIDEOOMME with  $T^*$ .** This plot visualizes the results for GPT-4o when refining the Top-32 output from  $T^*$ . The top-left region is optimal.

## C. Additional Visual Evidence for the Prevalence of ‘visual echoes’

To further demonstrate that ‘visual echoes’ are a pervasive challenge not limited to a specific video type, this section provides additional case studies. While our main paper (Figure 2) uses a simple animation to clearly illustrate the issue, here we show that the same pattern of severe frame redundancy occurs in more complex scenarios, including a scientific animation (Figure 10) and a real-world video with significant visual detail (Figure 11).

## D. Note on the AKS\* Baseline Adaptation

In our main experiments, we use *AKS\** as our primary sophisticated baseline. It is important to clarify the distinction between the original *AKS* framework [31] and our adapted *AKS\** version, and to justify this choice.

**Rationale for Adaptation.** Unlike other selectors such as  $T^*$  and *VSL*S that employ a direct Top-K selection, the

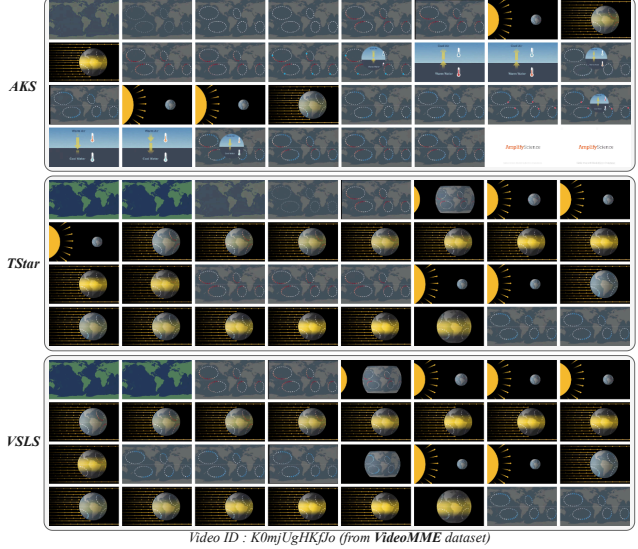


Figure 10. **Case Study 2: ‘Visual Echoes’ in a Scientific Animation Video.** This example (Video ID: K0mjUgHKfJo) shows that even in educational content with distinct conceptual phases, all three selectors produce highly repetitive frames of the Earth’s rotation and its position relative to the sun.



Figure 11. **Case Study 3: ‘Visual Echoes’ in a Real-World Video.** This example (Video ID: N1cdUjctpG8) demonstrates the prevalence of redundancy in complex, real-world footage. Despite challenging lighting and rich details, all selectors still select numerous near-identical shots of the same artifacts.

original *AKS* utilizes a more sophisticated **dynamic sampling algorithm**. This algorithm recursively allocates frame budgets to temporal segments based on score distributions. While innovative, this dynamic approach does not guarantee a fixed number of output frames (e.g., it may return 6 frames when a budget of 8 is requested), making rigorous,

Method	Avg. Fr.	Long(%)	Med. (%)	Short(%)
<i>Evaluation from Top 8 Keyframes</i>				
<b>Model: GPT-4o</b>				
$T^*$ Baseline	8.0	44.3	46.2	66.0
Uniform (Matched)	2.2	45.5	48.8	64.0
$T^*$ (Top-N, Matched)	2.2	46.4	<b>53.1</b>	64.0
<b>AFP</b> only (Ours)	2.2	<b>47.3</b>	48.8	68.0
<b>AFP + Graph</b> (Ours)	<b>2.2</b>	46.4	52.7	<b>80.0</b>
<b>Model: Qwen2.5-VL-7B-Instruct</b>				
$T^*$ Baseline	8.0	42.0	47.7	54.0
Uniform (Matched)	2.2	35.7	38.5	<b>70.0</b>
$T^*$ (Top-N, Matched)	2.2	<b>43.8</b>	<b>48.1</b>	56.0
<b>AFP</b> only (Ours)	2.2	38.7	41.9	66.0
<b>AFP + Graph</b> (Ours)	<b>2.2</b>	42.0	45.4	66.0
<b>Model: LLaVA-Video-7B-Qwen2</b>				
$T^*$ Baseline	8.0	42.0	47.7	44.0
Uniform (Matched)	2.2	40.8	46.5	48.0
$T^*$ (Top-N, Matched)	2.2	39.3	45.4	42.0
<b>AFP</b> only (Ours)	2.2	39.6	49.2	52.0
<b>AFP + Graph</b> (Ours)	<b>2.2</b>	<b>45.5</b>	<b>51.5</b>	<b>62.0</b>
<i>Evaluation from Top 32 Keyframes</i>				
<b>Model: GPT-4o</b>				
$T^*$ Baseline	32.0	53.1	48.8	74.3
Uniform (Matched)	4.2	46.4	48.8	62.0
$T^*$ (Top-N, Matched)	4.2	<b>49.1</b>	<b>55.0</b>	62.0
<b>AFP</b> only (Ours)	4.2	45.8	48.8	70.0
<b>AFP + Graph</b> (Ours)	<b>4.2</b>	48.5	53.1	<b>80.0</b>
<b>Model: Qwen2.5-VL-7B-Instruct</b>				
$T^*$ Baseline	32.0	38.7	41.9	40.0
Uniform (Matched)	4.2	38.1	43.5	64.0
$T^*$ (Top-N, Matched)	4.2	41.4	<b>48.5</b>	<b>68.0</b>
<b>AFP</b> only (Ours)	4.2	41.1	41.2	62.0
<b>AFP + Graph</b> (Ours)	<b>4.2</b>	<b>42.6</b>	43.1	<b>68.0</b>
<b>Model: LLaVA-Video-7B-Qwen2</b>				
$T^*$ Baseline	32.0	40.2	44.2	50.0
Uniform (Matched)	4.2	38.7	46.9	48.0
$T^*$ (Top-N, Matched)	4.2	<b>42.3</b>	46.9	48.0
<b>AFP</b> only (Ours)	4.2	41.1	49.2	44.0
<b>AFP + Graph</b> (Ours)	<b>4.2</b>	42.0	<b>52.7</b>	<b>62.0</b>

(a) Results on the LONGVIDEOBENCH dataset.

Method	Avg. Fr.	Long(%)	Med. (%)	Short(%)
<i>Evaluation from Top 8 Keyframes</i>				
<b>Model: GPT-4o</b>				
$T^*$ Baseline	8.0	51.3	51.5	55.2
Uniform (Matched)	2.1	50.1	54.2	58.6
$T^*$ (Top-N, Matched)	2.1	49.9	51.7	56.2
<b>AFP</b> only (Ours)	2.1	52.2	51.1	56.7
<b>AFP + Graph</b> (Ours)	<b>2.1</b>	<b>52.3</b>	<b>55.3</b>	<b>66.1</b>
<b>Model: Qwen2.5-VL-7B-Instruct</b>				
$T^*$ Baseline	8.0	<b>38.2</b>	38.3	43.1
Uniform (Matched)	2.1	37.7	39.4	42.5
$T^*$ (Top-N, Matched)	2.1	36.1	38.5	41.4
<b>AFP</b> only (Ours)	2.1	38.0	39.3	41.5
<b>AFP + Graph</b> (Ours)	<b>2.1</b>	36.2	<b>40.4</b>	<b>49.5</b>
<b>Model: LLaVA-Video-7B-Qwen2</b>				
$T^*$ Baseline	8.0	40.4	41.3	41.6
Uniform (Matched)	2.1	38.8	41.6	39.2
$T^*$ (Top-N, Matched)	2.1	39.3	41.0	38.8
<b>AFP</b> only (Ours)	2.1	37.8	40.4	40.0
<b>AFP + Graph</b> (Ours)	<b>2.1</b>	<b>42.3</b>	<b>46.2</b>	<b>56.1</b>
<i>Evaluation from Top 32 Keyframes</i>				
<b>Model: GPT-4o</b>				
$T^*$ Baseline	32.0	52.6	54.4	57.5
Uniform (Matched)	4.1	52.4	55.2	57.7
$T^*$ (Top-N, Matched)	4.1	49.8	49.4	54.6
<b>AFP</b> only (Ours)	4.1	51.8	53.6	55.7
<b>AFP + Graph</b> (Ours)	<b>4.1</b>	<b>52.6</b>	<b>55.3</b>	<b>63.1</b>
<b>Model: Qwen2.5-VL-7B-Instruct</b>				
$T^*$ Baseline	32.0	36.9	40.2	42.2
Uniform (Matched)	4.1	<b>39.9</b>	<b>43.1</b>	43.5
$T^*$ (Top-N, Matched)	4.1	37.9	40.1	43.4
<b>AFP</b> only (Ours)	4.1	39.6	40.4	44.6
<b>AFP + Graph</b> (Ours)	<b>4.1</b>	39.4	40.7	<b>52.3</b>
<b>Model: LLaVA-Video-7B-Qwen2</b>				
$T^*$ Baseline	32.0	38.2	42.2	41.6
Uniform (Matched)	4.1	38.7	42.9	41.3
$T^*$ (Top-N, Matched)	4.1	40.2	39.3	40.3
<b>AFP</b> only (Ours)	4.1	38.4	41.7	39.3
<b>AFP + Graph</b> (Ours)	<b>4.1</b>	<b>41.7</b>	<b>47.1</b>	<b>55.0</b>

(b) Results on the VIDEOMME dataset.

Table 4. **Generalizability study on the  $T^*$  selector.** This table shows the complete component-wise ablation results of applying our framework to the output of  $T^*$  on both datasets. **Bold** indicates the best performance among the four matched-budget strategies for each accuracy column.

fixed-budget comparisons challenging. To ensure a fair and reproducible evaluation protocol, we therefore modify its final stage to a standard Top-K selection.

Crucially, this choice is empirically supported by the ablation studies within the original AKS paper itself. Their experiments [31] show that a standard Top-K selection (denoted ‘TOP’) is the best performing alternative, achieving results highly competitive with their full adaptive method (‘ADA’) (e.g., 62.4% vs. 62.7% on LONGVIDEOBENCH). This confirms that our AKS\* adaptation, based on Top-K selection, serves as a powerful and faithful representation of the original method’s capabilities for the purpose of a strong

baseline comparison.

**Validity of the ‘Visual Echoes’ Motivation.** This modification does not weaken our core claim regarding the prevalence of ‘visual echoes’. The problem of frame redundancy is not an artifact of simple Top-K selection. As visually demonstrated in our qualitative examples (Figure 2 and Appendix C), ‘visual echoes’ are a fundamental challenge rooted in the temporal nature of video. The original, more complex dynamic sampling of AKS also suffers from this issue because if a temporal segment with high visual similarity

receives a high score, the algorithm will still allocate budget to select multiple, similar frames from within that segment. This reinforces our central argument: regardless of the final selection strategy, the ‘visual echoes’ problem persists, universally motivating the need for a dedicated refinement layer like our *AFP* framework.

## E. Further Implementation Details

This section provides in-depth details about our implementation to ensure full reproducibility of our work.

### E.1. AFP Algorithm Details

Our *Adaptive Frame-Pruning (AFP)* algorithm is implemented in Python using the scikit-learn library [24] for clustering. Below are the key implementation details that complement the description in the main paper’s Methodology section.

#### Clustering Parameters.

For the core clustering step, we use the `AgglomerativeClustering` class from scikit-learn. The `linkage` parameter, which determines the merge strategy, is set to ‘average’. This means the distance between two clusters is defined as the average of the distances between all pairs of samples, with one sample from each cluster.

#### Small Cluster Refinement.

To enhance the robustness of our clustering, we implement a refinement step (`refine_clusters` in our script). After the initial clustering, any cluster containing fewer than two frames is considered unstable. Such singleton clusters are merged into their nearest neighboring cluster, where proximity is determined by the average visual cosine distance between the frames of the two clusters. This prevents trivial clusters and ensures a more meaningful grouping.

#### Adaptive Threshold Calculation.

As mentioned in the main paper, the `distance_threshold` for clustering is determined adaptively. Specifically, after calculating all pairwise visual cosine distances, we fit a Gaussian Kernel Density Estimator (KDE) to their distribution. The threshold is then calculated as  $\tau = p + 0.15$ , where  $p$  is the distance value corresponding to the peak of the density function. The constant offset of 0.15 is an empirically chosen value designed to prevent the clustering from being overly conservative (i.e., creating too many small clusters) and to encourage the merging of closely related ‘visual echoes’.

## E.2. Prompt Structure and MLLM Inference

The structure of the prompts sent to the MLLM is critical for achieving consistent and reproducible results. In this section, we detail the two primary prompt templates used in our framework: one for our versatile semantic graph generation (Case 2), and one for the final downstream Video-QA task.

**Prompt for Semantic Graph Generation.** For our low-cost, universally applicable semantic graph generation strategy (Case 2), we employ a sophisticated prompt designed to elicit rich, structured information from the MLLM based solely on textual input. As detailed in Figure 12, the prompt is structured using several advanced prompting techniques:

- **Persona Prompting:** We assign the MLLM the role of an “expert visual scene analyst” to activate its advanced reasoning capabilities.
- **Chain-of-Thought Instructions:** The prompt provides a clear, step-by-step thinking process (Key Entity Identification, Contextual Cue Identification, Relationship Extraction) for the MLLM to follow.
- **Open-ended yet Structured Relation Extraction:** Crucially, our prompt encourages flexibility. It explicitly defines two categories of relations—Concrete (e.g., verbs, prepositions) and Abstract Logical (e.g., ‘spatial’, ‘causal’)—and provides clear examples and definitions for each. This “dual-track” design allows for the capture of a much richer and more nuanced set of semantic connections while maintaining a structured output.
- **Few-Shot Example:** A comprehensive example is provided to demonstrate the desired input-output format and the expected quality of the extracted graph.

The full prompt is shown in Figure 12.

**Prompt for Downstream Video-QA.** For the final question-answering stage, we utilize a clean, direct, and robust prompt template, detailed in Figure 13. This prompt is designed for maximum compatibility across different MLLMs. It clearly presents the visual evidence (via ‘<image>’ placeholders), followed by the optional textual semantic graph, and finally the question and multiple-choice options. The instructions are direct and unambiguous, strictly constraining the model to output a single uppercase letter corresponding to its chosen answer. This minimalist design minimizes prompt engineering sensitivity and ensures that performance differences are attributable to the quality of the visual and semantic inputs, rather than variations in prompt interpretation.

## E.3. Computational Environment

Our experiments were conducted within the computational environment detailed in Table 5. The deep learning models were implemented using the PyTorch framework [23].

## F. Analysis of Hyperparameters and Components

### F.1. Ablation Study on Prompt Formulation

The formulation of the prompt, particularly how the semantic graph is textualized and how instructions are given to the MLLM, can significantly impact performance. To determine the optimal prompt structure for our main experiments, we conducted an ablation study on several variants. All experi-

## The prompt template for LLM-based semantic graph generation

Here is a multiple-choice question based on a video. You are an expert visual scene analyst. Your task is to deconstruct the question and multiple-choice options to identify key entities and their relationships.

### Input:

- Question: {question\_text}
- Options: {options\_text}

### Instructions:

1. Key Entity Identification: From the Question and Options, extract 3-5 core entities (e.g., "person", "car") that are central to the query.
2. Contextual Cue Identification: Extract 2-4 additional scene elements that provide context or help locate the key entities.
3. Relationship Extraction: Infer all plausible relationships between the extracted entities.

A relationship MUST be a triplet '(Entity1; Relation; Entity2)'. The "Relation" can be one of two types:

- A) Concrete Relation: A concise verb or prepositional phrase describing a specific, physical action or state.  
Examples: 'wearing', 'holding', 'near', 'on top of', 'looking at'.
- B) Abstract Logical Relation: A word describing a fundamental logical connection between entities.

You are encouraged to infer such relations when applicable.

Examples & Definitions:

- a. spatial: Describes co-occurrence or positional arrangement (e.g., two objects in the same place).
- b. attribute: Describes a property of an entity (e.g., a person's clothing color).
- c. temporal: Describes a sequence in time (e.g., one event happens after another).
- d. causal: Describes a cause-and-effect link.
- e. functional: Describes the purpose or use of an object (e.g., a key is for a door).

Condition: Both entities in a triplet must be from the entities you extracted in steps 1 and 2.

### Output Rules:

1. Provide your response in three separate lines starting with the exact prefixes: 'Key Objects:', 'Cue Objects:', and 'Rel:'.
2. In the 'Key Objects:' and 'Cue Objects:' lines, separate items with a comma.
3. In the 'Rel:' line, separate each complete triplet '(...)' with a comma. Inside each triplet, separate the three elements with a semicolon.
4. Never use markdown or natural language explanations in your output.

### Example:

Input:

- Question: In a kitchen, after the woman in a red shirt opens the fridge with a key, what does she take out?
- Options: A) A bottle of milk, B) A green apple

### Response:

Key Objects: woman, red shirt, fridge, key, milk, green apple

Cue Objects: kitchen

Rel: (woman; attribute; red shirt); (woman; in; kitchen); (key; functional; fridge); (woman; opens; fridge); (fridge; temporal; milk)

Figure 12. **The full prompt template for LLM-based semantic graph generation.** This prompt leverages persona, chain-of-thought, and open-ended relation extraction to guide the LLM in deconstructing the query.

The prompt template for downstream Video-QA

Select the best answer to the following multiple-choice question based on the video.  
<image>  
<image>  
...  
[Here is an additional semantic graph context for this Video-QA]  
Objects in video context: <Objects>  
Relationships between objects: <Relations>  
Question: <Question>  
Options: <Options>  
Answer with the option's letter from the given choices directly.  
Your response format should be strictly an upper case letter A,B,C,D or E.

Figure 13. **The full MLLM prompt template used for the final Video-QA task.** It integrates image placeholders, the optional semantic graph, and the QA content into a single, direct query.

ments were performed on the LongVideoBench dataset with the GPT-4o model, starting from Top-8 keyframes.

### F.1.1. Prompt Component Variants

We tested combinations of two graph\_context formats and two system\_prompt formats:

#### Graph Context Formats.

- **Concise Triplet (G1):** Our final choice. This format is simple and structured, directly presenting nodes and

Component	Specification
Language	Python 3.9+
Deep Learning Framework	PyTorch
Key Libraries	scikit-learn, transformers, OpenCV
Conda Environment Name	VC
GPU	8x NVIDIA RTX A6000 (48GB VRAM each)
CUDA Version	12.1

Table 5. **Software and hardware environment for our experiments.**

raw triplet relationships (e.g., (object1, relation, object2)).

- **Verbose Natural Language (G2/G3):** These formats attempt to convert the graph into more human-like sentences (e.g., "object1 appears with object2").

#### System Prompt Formats.

- **Direct Prompt (P1):** Our final choice. This is a concise,

direct instruction for the QA task.

- **Instructional Prompt (P2):** This is a more verbose prompt that assigns an “expert” persona to the MLLM and provides detailed step-by-step guidelines.

### F.1.2. Results and Analysis

The results of our prompt ablation are presented in Table 6. **A “Less is More” Phenomenon in Prompting.** Interestingly, this ablation study reveals a microcosm of our paper’s central ‘Less is More’ theme, but applied to the prompt engineering space. As shown in Table 6, while more verbose and complex combinations like (G1, P2) or (G3, P2) can achieve marginally higher peak accuracy on specific video lengths (e.g., Short videos), this gain is inconsistent and comes at the cost of stability and increased token counts. The simpler, more direct (G1, P1) format demonstrates a superior balance across all metrics. This suggests that MLLMs can suffer from a form of “**instructional noise**” or “prompt dilution,” where overly elaborate instructions can sometimes obscure the core task, mirroring how excessive visual frames can cause “context dilution.”

Based on this finding, our analysis led us to select the combination of **Concise Triplet graph (G1)** and **Direct Prompt (P1)** for all main experiments, guided by the following key reasons:

- **Robust and Stable Performance:** While other combinations, such as (G1, P2), achieve marginally higher accuracy on certain video lengths, the (G1, P1) combination demonstrated the most stable and consistent high performance across all our preliminary and main experiments. As noted in our experimental logs, other verbose combinations frequently yielded unexpectedly low results in some runs, indicating a lack of robustness. The (G1, P1) setting, in contrast, reliably produced strong results.
- **Token Efficiency:** The G1 and P1 formats are significantly more concise than their verbose counterparts. This results in a lower token count for each query, which directly aligns with our paper’s core objective of maximizing token efficiency.
- **Simplicity and Generalizability:** The direct, structured format of (G1, P1) provides clear instructions to the MLLM without excessive “prompt engineering.” We believe this simpler format is more likely to generalize well across different MLLMs, as it relies on fundamental instruction-following capabilities rather than sensitivity to nuanced persona-based instructions.

In conclusion, our chosen (G1, P1) prompt formulation represents the best trade-off between performance, stability, and token efficiency, making it the most suitable choice for our proposed method.

## F.2. Analysis of Hyperparameters

This section provides the detailed data and analysis supporting our hyperparameter selection, ensuring the repro-

Graph Format	Prompt Format	Avg. Accuracy (%)		
		Long	Medium	Short
<b>G1 (Ours)</b>	<b>P1 (Ours)</b>	<b>47.0</b>	52.5	69.0
G2	P1	46.1	51.7	66.4
G1	P2	46.7	<b>52.9</b>	<b>70.7</b>
G2	P2	45.9	49.9	69.0
G3	P2	44.9	51.2	<b>70.7</b>

Table 6. **Ablation study on prompt formulation.** Results are averaged over multiple runs. Our chosen combination (G1, P1) is highlighted in **bold**.

ducibility of our work. Our method’s core hyperparameters, the feature fusion ratio  $\alpha$  and the distance metric weight  $\beta$ , were determined through a systematic sensitivity analysis. This analysis reveals a clear cost-utility trade-off, allowing our framework to be tuned to prioritize either performance (utility) or efficiency (cost).

All experiments were performed on the LONG VIDEOBENCH dataset using the Qwen2.5-VL-7B-Instruct model, starting from VSL5\* Top-8 keyframes. The results, averaged over multiple runs, are visualized in Figure 14 and detailed with exact values in Table 7.

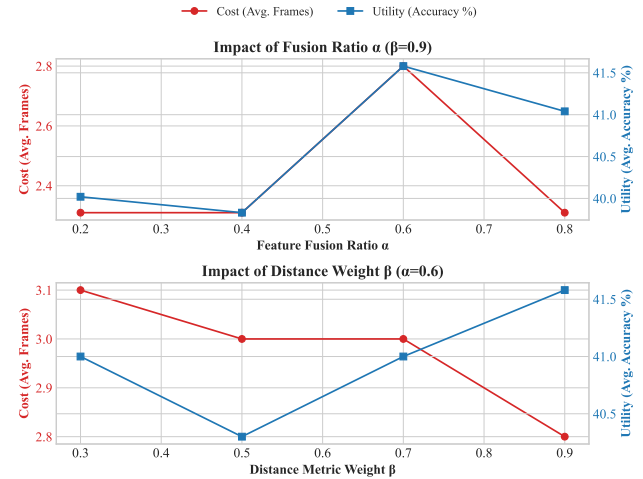


Figure 14. **Cost-Utility trade-off analysis for hyperparameters  $\alpha$  and  $\beta$ .** Cost (left y-axis, red) is measured by the average number of output frames, while Utility (right y-axis, blue) is measured by the average QA accuracy on a subset of LONGVIDEOBENCH. The plots demonstrate that our parameters are tunable knobs: users can adjust them to prioritize either higher accuracy (e.g., lower  $\beta$ ) or maximum efficiency (e.g., higher  $\beta$ ). Our default choice ( $\alpha = 0.6, \beta = 0.9$ ) represents a strong balance.

**Analysis and Selection Strategy.** As visualized in Figure 14 and detailed in Table 7, our analysis reveals a clear cost-utility trade-off. For the feature fusion ratio  $\alpha$ , the results show that  $\alpha = 0.6$  achieves the highest average accuracy of 41.58%, suggesting an optimal balance between

Hyperparameter Setting	Avg. Accuracy (%)	Avg. Frames
<i>Analysis of Feature Fusion Ratio <math>\alpha</math> (fixing <math>\beta = 0.9</math>)</i>		
$\alpha = 0.2$	40.02	<b>2.31</b>
$\alpha = 0.4$	39.83	<b>2.31</b>
<b><math>\alpha = 0.6</math> (Ours)</b>	<b>41.58</b>	2.80
$\alpha = 0.8$	41.04	<b>2.31</b>
<i>Analysis of Distance Metric Weight <math>\beta</math> (fixing <math>\alpha = 0.6</math>)</i>		
$\beta = 0.3$	41.00	3.10
$\beta = 0.5$	40.30	3.00
$\beta = 0.7$	41.00	3.00
<b><math>\beta = 0.9</math> (Ours)</b>	<b>41.58</b>	<b>2.80</b>

Table 7. **Detailed sensitivity analysis of hyperparameters  $\alpha$  and  $\beta$ .** Results are averaged over multiple runs on the LONG VIDEOBENCH dataset using the Qwen2.5-VL-7B-Instruct model (from Top-8). Our chosen parameters ( $\alpha = 0.6, \beta = 0.9$ ) are highlighted in **bold**.

visual and semantic features, albeit at a slightly higher frame cost. For the distance metric weight  $\beta$  (bottom plot), a higher value (e.g., 0.9) leads to more aggressive clustering (fewer frames, as shown by the red line) and, in this case, also yields the highest accuracy.

This demonstrates that the hyperparameters of **AFP** are not arbitrary fixed values, but rather tunable “knobs” that control the cost-utility balance. Based on this systematic analysis, we selected the configuration of  $\alpha = 0.6$  and  $\beta = 0.9$  for all main experiments, as it consistently provided the best overall performance and a favorable efficiency-accuracy balance in our development set.

### F.3. Representative Frame Selection Strategy

A crucial step in our **AFP** algorithm is selecting a single representative frame from each generated cluster. To determine the most effective and robust approach, we conducted a comprehensive ablation study comparing three distinct strategies. The experiments were performed on the LONG VIDEOBENCH dataset with the GPT-4o model, starting from Top-8 keyframes provided by **VSLS\***, and the results reported are averaged over multiple runs to ensure reliability. This analysis focuses on the ‘**AFP** only’ setting (without the semantic graph) to purely evaluate the quality of the selected visual information.

- **Score-based (Highest **VSLS\*** Score):** This strategy leverages external information by selecting the frame from each cluster that has the highest initial relevance score assigned by the upstream **VSLS\*** selector.
- **Centroid-based (Visual Centroid):** This strategy is self-contained. It selects the “centroid frame”—the frame with the minimum average feature distance to all other frames within the same cluster, making it the most visually representative.

- **Relevance-based (Highest Query Similarity):** This strategy introduces task-specific guidance by selecting the frame with the highest CLIP similarity score to the ‘Question + Options’ text prompt.

As shown in Table 8, the averaged results over multiple runs confirm that the **Centroid-based strategy** holds a clear advantage. It achieves the highest overall accuracy (48.53%), outperforming both the Score-based and Relevance-based approaches.

The superiority of the Centroid strategy is theoretically sound, especially in the absence of a semantic graph. By selecting the frame closest to the cluster’s feature-space center, it guarantees the most visually representative frame is chosen, which is the most robust way to minimize information loss during the pruning process. This self-contained logic is arguably more generalizable than relying on external scores (from **VSLS\*** or CLIP), which might be noisy or biased. Based on these comprehensive findings, we adopted the **Centroid-based strategy** for all main experiments reported in this paper.

## G. Qualitative Analysis and Limitations

### G.1. Additional Qualitative Examples

To demonstrate the versatility and robustness of our **Adaptive Frame-Pruning (AFP)** method, this section provides qualitative examples from diverse Video-QA tasks. These cases illustrate how **AFP** effectively handles various forms of visual redundancy while preserving the crucial information needed to answer different types of queries.

**Example 1: Motion Recognition.** Figure 15 presents a challenging task requiring the identification of a fast-moving object based on a descriptive, distractor-rich query. The baseline **VSLS\*** method, aiming for comprehensive coverage, selects 16 keyframes. However, these frames are plagued by severe ‘visual echoes’: the first twelve frames are nearly identical, capturing a static view of an ambulance. This flood of repetitive information risks overwhelming the MLLM.

Our **AFP** algorithm excels in such scenarios. It correctly identifies and merges the redundant static and slightly shifted shots into distinct representative frames. Consequently, the input is drastically reduced to a highly efficient set of just 3 frames. By capturing the ambulance’s initial state, a subtle movement, and the surrounding context, these frames preserve the critical temporal cues needed to infer motion. This compact visual input, augmented by the textual semantic graph, provides a sufficient, non-redundant context for the MLLM to correctly identify the “Ambulance”.

**Example 2: Counting Task.** Figure 16 showcases a counting-based question: “How many porcelain jars were discovered...?”. To answer this, the model must identify and aggregate all visible jars. The baseline **VSLS\*** selector, in its effort to be comprehensive, retrieves 32 keyframes. Among

Experimental Settings				Averaged Results	
Dataset	Model	Frame Source	Selection Strategy	Avg. Acc (%)	Avg. Frames
LONGVIDEOBENCH	GPT-4o	VSL*	Score-based	47.14	2.1
			<b>Centroid-based</b>	<b>48.53</b>	<b>2.1</b>
			Relevance-based	46.67	2.2

Table 8. **Ablation study on representative frame selection strategies.** The experiment was conducted in the ‘*AFP* only’ setting to purely evaluate the quality of the selected visual information. Results are averaged over multiple runs. The Centroid-based strategy demonstrates the best performance.

## Motion Recognition

**Query:** Among the many vehicles and crowded places, with white lights on the left, a tent on the right, and an ambulance with yellow lights in the distance, which object is moving quickly?

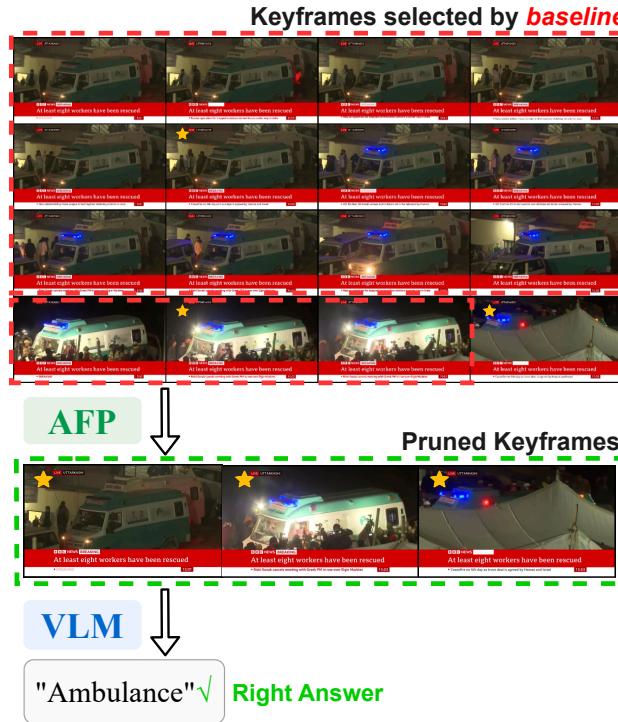


Figure 15. Qualitative example for a **motion recognition task** (Video ID: Z00vWImw1KQ). The query asks to identify a moving object. The baseline *VSL\** selects 16 frames with high redundancy. Our *AFP* algorithm prunes this set to just 3 frames that preserve the key motion cues, enabling the MLLM to derive the correct answer.

these, at least seven frames capture the porcelain jars from slightly different but highly overlapping angles, creating significant redundancy. Our *AFP* algorithm correctly identifies these frames as a single ‘visual echo’. It merges these seven redundant views into a single, clear representative frame that encapsulates the essential information for counting. By

combining this consolidated view with three other contextually important (but non-redundant) frames, *AFP* reduces the input from 32 to just 4 frames. This compact set is sufficient for the MLLM to correctly answer “9”, demonstrating how our method eliminates noise while preserving the core evidence required for aggregation tasks.

**Example 3: Fine-Grained Detail Recognition.** Figure 17 illustrates a more challenging task requiring the recognition of fine-grained details—specifically, small text in the query “What level of magnification is used...?”. The crucial text “2000x magnification” appears in multiple early frames. The *VSL\** baseline selects 30 frames, with the first six being almost perfect duplicates. A naive de-duplication might aggressively merge all six into one. However, our *AFP* algorithm demonstrates a more nuanced approach. It prunes the 30 initial frames down to just 3. Critically, among these three, it preserves *two* of the initial six frames. This is because subtle changes in focus or cellular movement create enough feature variance for our adaptive clustering to treat them as distinct (though closely related) pieces of evidence. This intelligent, slightly conservative pruning proves highly effective: it drastically reduces redundancy while increasing the robustness of the final answer by providing the MLLM with multiple opportunities to spot the critical, fine-grained text. This case highlights that *AFP* does not merely de-duplicate, but rather optimizes the trade-off between redundancy reduction and evidence preservation.

## G.2. Discussion of Limitations

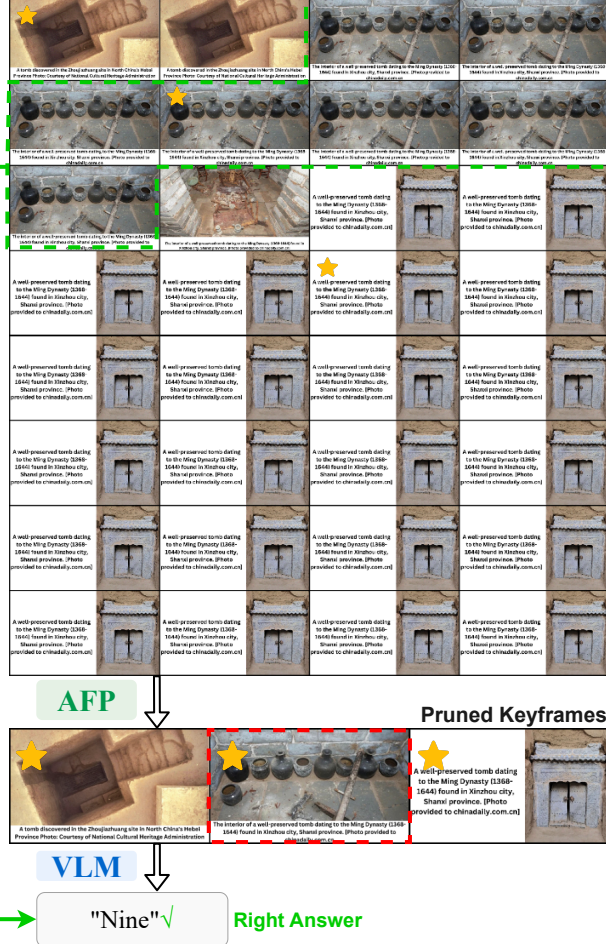
To provide a balanced perspective on our work, this section honestly discusses the inherent limitations of our proposed method and analyzes two representative failure cases. We believe this discussion is crucial for understanding the boundaries of our approach and for inspiring future research in efficient video understanding. Our approach, while effective, is subject to two limitations:

- **Dependency on Redundancy.** The core premise of *Adaptive Frame-Pruning (AFP)* is the existence of visual redundancy in the initial keyframe set. In scenarios featuring highly dynamic, non-repetitive content, such as a montage of rapidly changing scenes, the opportunities for clustering are naturally diminished. In such cases, *AFP* would cor-

## Counting Task

**Query:** How many porcelain jars were discovered in the niches located in the primary chamber of the tomb?

### Keyframes selected by *baseline*



## Detail Task

**Query:** What level of magnification is used to view the cells in the video??

### Keyframes selected by *baseline*

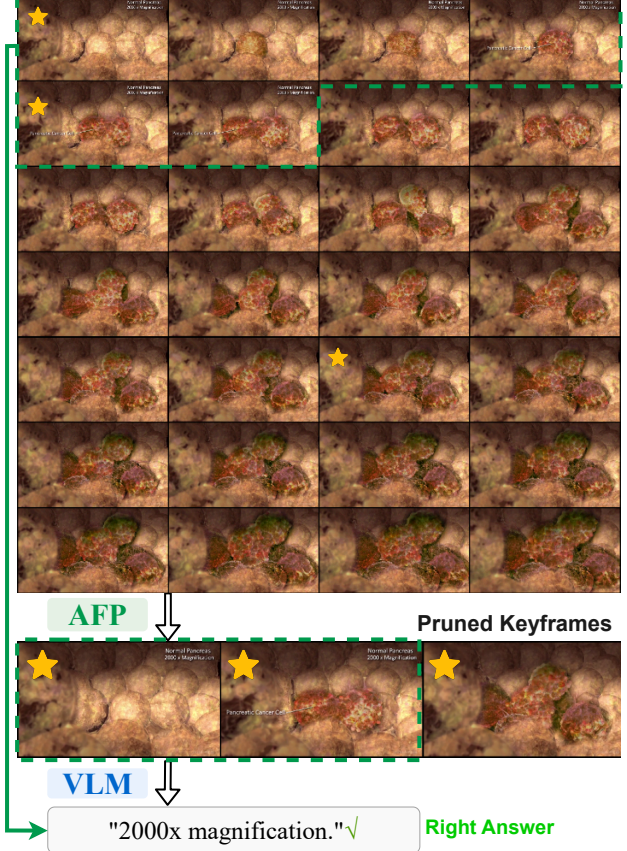


Figure 16. Qualitative example for a **counting task** (Video ID: N1cdUjctpG8). The query asks for the number of porcelain jars. The baseline *VSLS\** method selects 32 frames, many of which are redundant, capturing similar views of the jars. Our *AFP* algorithm prunes this set to just 4 frames by consolidating repetitive views, enabling the MLLM to perform an accurate count with a highly efficient prompt.

rectly identify most frames as unique and perform minimal reduction, thus offering limited efficiency gains.

• **Ceiling Effect from Upstream Selector.** Our method operates as a post-processing refinement layer. Consequently, its performance is fundamentally capped by the quality of the initial keyframe set provided by the upstream selector (e.g., *VSLS\**). If the initial selector fails to retrieve the frames containing the necessary evidence to answer a question, *AFP* cannot recover this information, as its role is to prune, not to discover.

Figure 17. Qualitative example for a **fine-grained detail recognition task** (Video ID: XWfqBKeC0g8). The query requires identifying small text within the frame. *VSLS\** selects 30 frames, with the first six being nearly identical. Our *AFP* intelligently prunes this to 3 frames, critically retaining two distinct frames that both contain the “2000x” text, ensuring this vital but subtle information is preserved for the MLLM.

### G.3. Failure Case Analysis

Beyond general limitations, we present two failure cases that highlight specific challenges.

**Case 1: Loss of Fine-Grained Information during Pruning.** The first case, shown in Figure 18, demonstrates a scenario where our *AFP* algorithm, while correctly identifying visual similarity, inadvertently discards critical, fine-grained information. The question asks which of human’s ancestors first began to walk on two legs. The initial 32 frames selected by *VSLS\** correctly contain frames depicting both “*Ramapithecus*” (the correct answer, appearing earlier) and “*Ardipithecus Ramidus*”. However, because the overall visual composition of these frames—the posture of the ancestor,

## Loss of Information

**Query:** According to the video, in which state did human's ancestors first begin to walk on two legs?

Keyframes selected by **baseline**

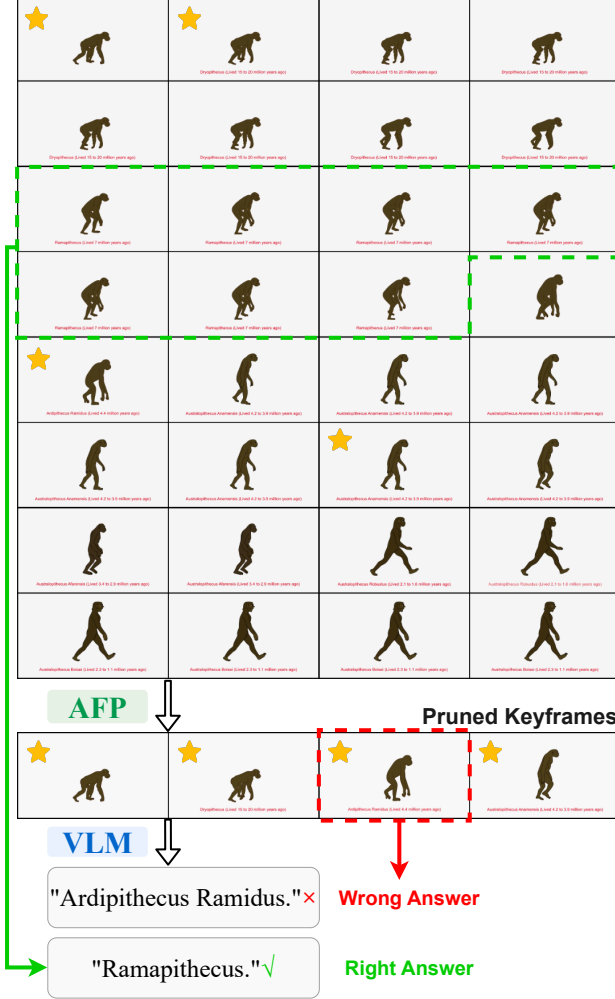


Figure 18. An analysis of a failure case caused by **information loss during pruning**. The initial keyframes from *VSLS\** contain the evidence for the correct answer “Ramapithecus” (highlighted in green). However, due to high visual similarity with other frames, our **AFP** algorithm incorrectly prunes this crucial frame, leading the VLLM to a wrong answer based on the remaining evidence.

the background—is highly similar, our algorithm, which relies on global ResNet and CLIP features, perceives them as a single ‘visual echo’. Consequently, it merges them into one cluster and, in this instance, retains only the frame for “Ardipithecus Ramidus”. The MLLM, presented with this incomplete evidence, understandably arrives at the wrong conclusion. This failure highlights a key limitation: our global feature-based approach can be insensitive to subtle but semantically decisive local details, such as small pieces of text. This points towards a clear avenue for future im-

## Insufficiency of Selector

**Query:** According to the video, which of the following is the main reason why people commemorate Qu Yuan?

Keyframes selected by **baseline**

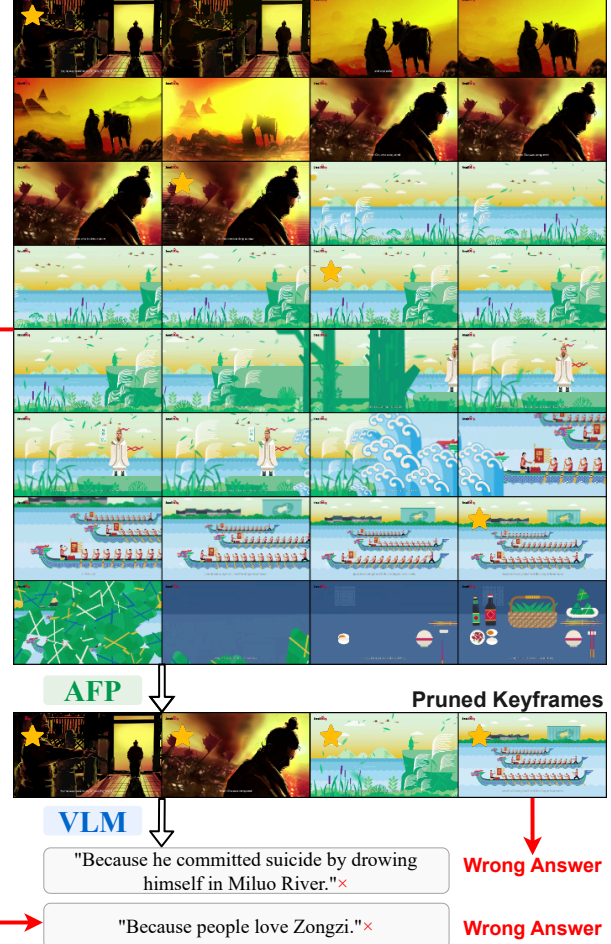


Figure 19. An analysis of a failure case caused by the **insufficiency of the upstream selector**. The question requires a global understanding of a narrative. The initial 32 frames from *VSLS\** are already insufficient to answer correctly. Our **AFP** method, while efficiently pruning the input, cannot recover the missing information, leading to an inevitable failure by the VLLM. This illustrates the performance ceiling imposed by the initial keyframe selection.

provement: integrating more localized feature extractors, such as Optical Character Recognition (OCR) models, into the clustering process.

**Case 2: Insufficiency of the Upstream Selector.** The second case, shown in Figure 19, exemplifies the “Ceiling Effect” limitation. The question asks for the *main reason* people commemorate Qu Yuan, a query that requires a deep, holistic understanding of a narrative spread across the entire video, likely conveyed through multiple subtitles. The initial 32 frames selected by *VSLS\**, while topically relevant, fail to

capture the full narrative context required to make such a nuanced judgment. As a result, even before our **AFP** algorithm is applied, the provided visual information is insufficient for the MLLM to correctly answer the question. After our method prunes the already insufficient set of frames, the MLLM still fails. This case clearly demonstrates that our method’s success is contingent on the upstream selector providing a set of frames that, even if redundant, collectively contains the necessary information. It highlights a broader challenge for all sparse sampling methods when dealing with questions that require global, narrative-level reasoning.

**Summary and Future Directions.** The comprehensive failure case analysis presented above provides invaluable insights into the inherent limitations of our framework and illuminates promising avenues for future research.

The first failure case, *Loss of Fine-Grained Information during Pruning*, highlights a primary weakness of our current **AFP** module: its reliance on **global visual features**. While this global perspective is highly effective for identifying broad ‘visual echoes’, it can sometimes be insensitive to subtle but semantically decisive local details, such as small pieces of text (e.g., “*Ramapithecus*” vs. “*Ardipithecus Ramidus*”). Our algorithm’s tendency to merge these visually similar frames into a single cluster underscores a fundamental trade-off between redundancy reduction and evidence preservation. This points towards a clear future direction: developing an **adaptive feature fusion mechanism**. Such a system could initially perform a global clustering to efficiently handle large-scale redundancy. Subsequently, for clusters that are visually similar but potentially detail-rich, it could dynamically switch to a more **localized, patch-based feature representation** or even incorporate an OCR model for re-evaluation, ensuring that critical fine-grained information is not inadvertently discarded.

The second failure case, *Insufficiency of the Upstream Selector*, perfectly exemplifies the “**Ceiling Effect**” and reinforces a central thesis of our main paper. Our framework is designed as a **refinement layer**, not a discovery tool. Its success is therefore fundamentally contingent on the upstream selector providing a set of frames that, even if redundant, collectively contains the necessary information. This case clearly demonstrates that if the initial keyframe set is already insufficient, our method, while still performing its pruning task efficiently, cannot magically recover the missing narrative context. This highlights a broader challenge for all sparse sampling methods when dealing with questions that require global, narrative-level reasoning.

Ultimately, both failure cases point towards a unified future vision that we briefly touch upon in our conclusion: the development of a ‘**Multimodal Semantic Graph**’. Such a compact, structured representation could potentially serve as a more holistic proxy for the entire video. By encapsulating not just textual relationships, but also key visual motifs (like

the subtle difference between two ancestors), audio cues, and crucial textual information from subtitles or OCR, it could offer a more robust and token-efficient foundation for long-form video understanding. This would shift the paradigm from merely “selecting better frames” to “building a better, comprehensive understanding” of the video content, paving the way for more robust and scalable video AI.